

# Spatial distributions of core-collapse supernovae in infrared-bright galaxies

T. Kangas,<sup>1,2\*</sup> S. Mattila,<sup>3</sup> E. Kankare,<sup>3</sup> J. K. Kotilainen,<sup>3</sup> P. Väisänen,<sup>4,5</sup> R. Greimel<sup>6</sup> and A. Takalo<sup>1</sup>

<sup>1</sup>*Tuorla Observatory, Department of Physics and Astronomy, University of Turku, Väisäläntie 20, FI-21500 Piikkiö, Finland*

<sup>2</sup>*Nordic Optical Telescope, Apartado 474, E-38700 Santa Cruz de La Palma, Spain*

<sup>3</sup>*Finnish Centre for Astronomy with ESO (FINCA), University of Turku, Väisäläntie 20, FI-21500 Piikkiö, Finland*

<sup>4</sup>*South African Astronomical Observatory, PO Box 9, 7935 Observatory, Cape Town, South Africa*

<sup>5</sup>*South African Large Telescope, PO Box 9, 7935 Observatory, Cape Town, South Africa*

<sup>6</sup>*Institut für Physik, Universität Graz, Universitätsplatz 5/II, A-8010 Graz, Austria*

Accepted 2013 September 25. Received 2013 September 24; in original form 2013 May 7

## ABSTRACT

We have measured the correlation between the locations of core-collapse supernovae (CCSNe) and host galaxy light in the H $\alpha$  line, near ultraviolet (NUV), *R* band and *K*<sub>s</sub> band to constrain the progenitors of CCSNe using pixel statistics. Our sample consists of 86 CCSNe in 57 infrared (IR)-bright galaxies, of which many are starbursts and 10 are luminous infrared galaxies (LIRGs). We also analyse the radial distribution of CCSNe in these galaxies, and determine power-law and exponential fits to CCSN surface density profiles. To probe differences between the SN population of these galaxies and normal spiral galaxies, our results were compared to previous similar studies with samples dominated by normal spiral galaxies where possible. We obtained a normalized scale length of  $0.23^{+0.03}_{-0.02} R_{25}$  for the surface density of CCSNe in IR-bright galaxies; less than that derived for CCSNe in a galaxy sample dominated by normal spiral galaxies ( $0.29 \pm 0.01$ ). This reflects a more centrally concentrated population of massive stars in IR-bright galaxies. Furthermore, this centralization is dominated by a central excess of Type Ibc/IIb SNe. This may be due to a top-heavy initial mass function and/or an enhanced close binary fraction in regions of enhanced star formation. Type Ic SNe are most strongly correlated with H $\alpha$  light and NUV-bright regions, reflecting the shortest lifetime and thus highest mass for Type Ic progenitors. Previous studies with samples dominated by normal spiral galaxies have indicated a lower Ibc–H $\alpha$  correlation than our results do, which may be due to the central excess of Type Ibc/IIb SNe in our sample. The difference between Types II and Ib is insignificant, suggesting that progenitor mass is not the dominant factor in determining if a SN is of Type Ib or II. Similar differences in correlation can be seen in the *K*<sub>s</sub> band (which in these galaxies is dominated by red supergiants and thus also traces recent star formation), with Type Ibc/IIb SNe tracing the *K*<sub>s</sub>-band light better than Type II in our sample.

**Key words:** supernovae: general – galaxies: star formation – galaxies: statistics.

## 1 INTRODUCTION

Despite decades of ever-intensifying research on supernovae (SNe), our understanding of their exact origins still remains incomplete. The connection between the observed properties of core-collapse supernovae (CCSNe) and the properties of their progenitors is one of the questions of interest, in particular the differences between the progenitors of different SN types; whether the stellar mass is the dominant parameter or whether other factors such as binarity,

rotation or metallicity of the progenitor also contribute significantly (e.g. Smartt 2009; Smith et al. 2011; Eldridge et al. 2013, and references therein).

SNe are classified into two main types: Type I, with no hydrogen lines in their spectra; and Type II, whose spectra show these lines (e.g. Filippenko 1997). SNe of Types Ib, Ic (together referred to as Type Ibc) and II, i.e. CCSNe, are thought to have their origin in massive stars ( $\geq 8 M_{\odot}$ ; Smartt 2009) that explode after exhausting their nuclear fuel. The progenitors of Type Ibc and IIb SNe are thought to be massive stars that have lost their outer envelopes (H envelope for Ib and both H and He for Ic) by stellar winds or through mass transfer to a binary companion (see e.g. Eldridge et al.

\* E-mail: tjakan@utu.fi

2013). The progenitors of other Type II SNe, on the other hand, are believed to be less massive supergiant stars that have retained their envelopes. However, the nature of Type IIn SN progenitors is unclear. At least part of them are believed to be extremely massive stars (e.g. Smith et al. 2011), but Anderson et al. (2012, hereafter A12) instead found evidence that, on average, Type IIn SNe originate from the lower mass end of the CCSN progenitors.

Attempts to directly observe CCSN progenitors in pre-explosion archive images of host galaxies have yielded direct detections of several SN II progenitors (e.g. Smartt et al. 2004; Li et al. 2006; Mattila et al. 2008; Maund et al. 2011; Van Dyk et al. 2011), but the need to be able to resolve individual stars in other galaxies typically requires a space telescope or adaptive optics. Another way to study the progenitors is to observe the environments of the SNe. Statistical analysis of galaxy light close to the locations of historical SNe can yield constraints on the nature of their progenitors.  $H\alpha$  line emission is important in this context, since it traces regions of ionized hydrogen; and only massive young stars (that also give rise to CCSNe) contribute significantly to the ionizing radiation (Kennicutt 1998).

James & Anderson (2006) found an excess of Type II SNe in regions of low star-forming activity in contrast to SNe of Type Ibc by studying a sample of 63 SNe (of which, however, 25 were either of Type Ia or had no designated type). This analysis was repeated for a total of 260 SNe in Anderson & James (2008, hereafter referred to as A08) and A12 with similar results. These results implied a mass sequence for CCSN progenitors running, in ascending order, from Type II through Ib to Ic. Kelly & Kirshner (2012) also argue for a higher mass for Type Ibc progenitors than Type II using colours of SN environments. In addition, statistical studies of the radial distribution of CCSNe have indicated that Type Ibc SNe are more centrally concentrated than Type II SNe (e.g. Petrosian et al. 2005; Prieto, Stanek & Beacom 2008; Anderson & James 2009; Hakobyan et al. 2009). In particular, this also appeared to be the case for disturbed galaxies, with presumably higher star formation rates (SFR) than in normal spiral galaxies (Habergham, Anderson & James 2010; Habergham, James & Anderson 2012).

Anderson, Habergham & James (2011) studied a single interacting luminous infrared galaxy (LIRG; defined as a galaxy with  $L_{IR} \geq 10^{11} L_{\odot}$ ) system, Arp 299 (NGC 3690 and IC 694), which has hosted seven optically observed SNe. They found evidence that its population of SNe may be different from that of normal spiral galaxies – with an abnormal number of stripped-envelope SNe abnormally close to the cores of the system – although the study has to deal with small-number statistics. One possible interpretation is that, because of the young age of the most recent starburst episode in the system, insufficient time has elapsed for the observed SN rates to reflect the SFRs for the full range of stellar masses capable of producing CCSNe  $\gtrsim 8 M_{\odot}$ . This lends support to Type Ibc and Ib SNe arising from progenitors of shorter lifetime than other Type II. On the other hand, the centralization of Type Ib/Ib SNe compared to other Type II in Arp 299 – and the central excess of Type Ibc SNe found in other studies – implies that in the central region with enhanced star formation, the initial mass function (IMF) may favour high-mass stars. According to Hakobyan et al. (2009), the central excess found in normal spiral galaxies can alternatively be explained by higher metallicities of the progenitors of Type Ibc SNe. Habergham et al. (2010, 2012) studied the central excess of Type Ibc SNe in disturbed galaxies, considering also metallicity as a possible explanation, but found this possibility unlikely.

The studies of e.g. James & Anderson (2006) (as well as A08 and A12) and Hakobyan et al. (2009) mentioned above concern

SNe in spiral galaxy hosts in general. In light of the recent results of Anderson et al. (2011), we study CCSNe in infrared (IR)-bright galaxies in a similar way in this paper. Our goal is to find out whether the SN and thus progenitor star population in these galaxies really differ from normal spiral galaxies. We apply the methods used by James & Anderson (2006) (and in subsequent papers), extending them to the  $R$  and  $K_s$  bands and to the near-UV. We also apply the method of Hakobyan et al. (2009). The results are then compared to the earlier studies. The paper is arranged as follows: in Section 2 we describe our sample and observations; Section 3 presents our data reduction methods; Sections 4 and 5 cover the statistical tools at our disposal and an overview of our results based on each method, respectively; in Section 6, we discuss our results; and finally, in Section 7, we present our conclusions.

## 2 SAMPLE AND OBSERVATIONS

A sample of IR-bright galaxies was selected from among those in the *IRAS* Revised Bright Galaxy Catalog (Sanders et al. 2003) based on their far-IR luminosities ( $L_{FIR}$ , in the wavelength range of 40–400  $\mu\text{m}$ ) and distance following the criteria below. Far-infrared luminosity was used as a criterion since it is a good tracer of star formation in actively star-forming galaxies. Luminosities and distances were taken from Sanders et al. (2003). The value for the Hubble constant used in this catalogue was  $75 \text{ km s}^{-1} \text{ Mpc}^{-1}$ .

- (1)  $d < 75 \text{ Mpc}$ ,
- (2)  $L_{FIR} > 1.6 \times 10^{10} L_{\odot}$  ( $\log L_{FIR} > 10.2$ ).
- (3) Type I Seyfert galaxies listed in Véron-Cetty & Véron (1998) were excluded to avoid contamination by an active galactic nucleus (AGN).
- (4) Observable from La Palma with a reasonable airmass, i.e.  $\text{Dec.} \gtrsim -35^{\circ}$ .

Habergham et al. (2012) argue that after  $cz > 6000 \text{ km s}^{-1}$  one will begin to miss SNe with low projected distance from the galaxy core. With our distance limit, this value is not exceeded by any host galaxy. The limit in  $L_{FIR}$  is roughly half of that of the ‘prototypical’ starburst galaxy, M82, in order to include a larger number of galaxies that still have high SFRs. It corresponds to a SFR of  $\sim 2.7 M_{\odot} \text{ yr}^{-1}$  according to equation (4) in Kennicutt (1998) and a CCSN rate of  $\sim 0.04 \text{ yr}^{-1}$  according to equation (1) in Mattila & Meikle (2001). The median distance in the sample is  $\sim 36 \text{ Mpc}$  and the median  $L_{FIR}$  is  $3.7 \times 10^{10} L_{\odot}$ . A comparison between our galaxy sample and that of A08/A12 is presented in Fig. 1 to show the different distance and luminosity ranges covered. The majority of the A08/A12 sample is well below our luminosity limit.

Any SNe discovered before 1990 were excluded from the sample. These SNe mostly had no (sub)type classification, and their exact coordinates were considered possibly inaccurate because they were often discovered using photographic plates. The coordinates of the SNe were obtained from the Asiago supernova catalogue (Barbon, Cappellaro & Turatto 1989).<sup>1</sup> All SNe of Type Ia were also excluded, since they arise from a much older stellar population than CCSNe and are thus outside the scope of this paper. This resulted in a total sample of 57 galaxies, 22 of which are brighter in the FIR than M82, the prototypical starburst galaxy, and 10 of which are LIRGs. The galaxy sample was sorted into three classes by eye, based on the presence or lack of tidal features or companion galaxies within a few arcminutes: isolated (28 galaxies), ‘disturbed’ (19 galaxies)

<sup>1</sup> <http://heasarc.gsfc.nasa.gov/W3Browse/all/asiagosn.html>

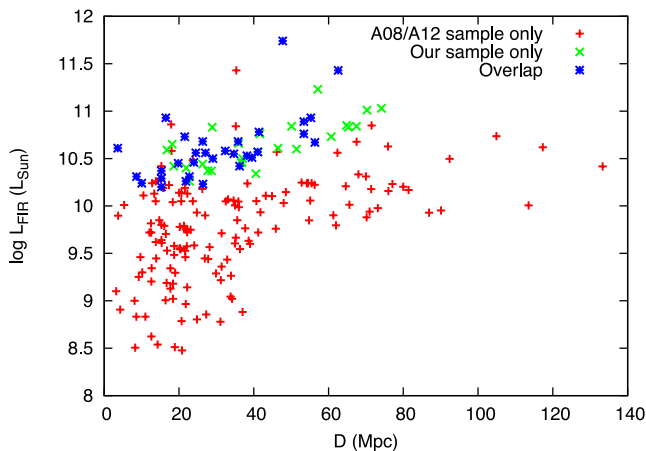


**Figure 1.** A comparison between the luminosities and distance ranges of our host galaxy sample and that of A08 and A12.

and merger/close pair (10 galaxies). The SN sample consists of 86 SNe, of which 35 were of Type Ib, Ic or IIb [*stripped-envelope SNe (SE-SNe)*]; 47 were of other Type II (II-P, II-L, II-n and those only classified ‘II’); and four were of undetermined type. For a complete list of CCSN host galaxies included in the study, see Table 1.

These galaxies were observed with the 2.56 m Nordic Optical Telescope (NOT) on La Palma, in the Canary Islands, using the Andalucía Faint Object Spectrograph and Camera (ALFOSC) instrument over several observing runs between 2009 and 2013. ALFOSC has a  $2048 \times 2048$  pixel detector, with a 0.19 arcsec pixel scale and a field of view (FOV) of  $6.4 \times 6.4$  arcmin<sup>2</sup>. Integration times for H $\alpha$  on- and off-filter images were between 300 and 600 s, depending on target brightness. H $\alpha$  on- and off-filters were selected based on the redshift of the galaxy (either at 661.0 nm, for redshifts under 0.0103, or 665.3 nm for the remaining galaxies) and usually the on-filter includes the [N II] line as well. *R*-band images for the sample were obtained using an exposure time of 100 s.

*Ks*-band images for a majority of the sample were obtained using the NOT near-infrared Camera and spectrograph (NOTCam), which has a  $1024 \times 1024$  pixel array, pixel scale of 0.234 arcsec and an FOV of  $4 \times 4$  arcmin<sup>2</sup> in wide-field imaging mode. The images were taken with a nine-point dither pattern on-source and one minute of integration time per pointing. The rest of the *Ks*-band images of the sample galaxies were obtained with the 4.2 m *William Herschel Telescope (WHT)*, using the Isaac Newton Group Red Imaging Device (INGRID; Packham et al. 2003) or Long-slit Intermediate Resolution Infrared Spectrograph (LIRIS; Manchado et al. 2004) instruments, as a part of a near-IR SN search programme (see Mattila, Meikle & Greimel 2004). INGRID has a  $1024 \times 1024$  pixel array, with a 0.24 arcsec pixel scale and an FOV of  $4.2 \times 4.2$  arcmin<sup>2</sup>; while LIRIS has a  $1024 \times 1024$  pixel array and a scale of 0.25 arcsec yielding an FOV of  $4.27 \times 4.27$  arcmin<sup>2</sup>. The *WHT* images were taken using a four-quarter dither pattern. The median seeing (full width at half-maximum; FWHM) of the optical, *Ks*-band and *GALEX* images in the sample are 1.0, 0.8 and 4.8 arcsec, corresponding to roughly 170 pc, 140 pc and 830 pc at our median distance of 36 Mpc, respectively.

The H $\alpha$  and *R*-band images for a few galaxies from Sánchez-Gallego et al. (2012) that matched our criteria were kindly shared by the authors: NGC 3034 (M82), NGC 3627 (M66), NGC 5194 (M51) and NGC 4041. These galaxies had been observed with the Kitt Peak 2.1 m (KP) telescope. For the Kitt Peak H $\alpha$  images, a filter centred at 657.3 nm was used. In addition, the optical images

of NGC 2146 were observed at the 2.5 m Isaac Newton Telescope (INT) with the Wide Field Camera (WFC), using an H $\alpha$  filter centred at 656.8 nm.

Near-ultraviolet (NUV) images were obtained from the *GALEX* space telescope data archive.<sup>2</sup> These images have a pixel scale of 1.5 arcsec, roughly four times that of the  $2 \times 2$  binned NOT/ALFOSC images used for this study, and a wavelength range of 177–273 nm. *GALEX* data were not available for five galaxies in our sample: NGC 6000, NGC 6643, NGC 6745, UGC 3829 and ESO 492-G02.

### 3 DATA REDUCTION

The NOTCam *Ks*-band images were taken with a nine-point ( $3 \times 3$ ) dither pattern. The sky-subtracted images were de-dithered and median combined. The *Ks*-band images taken with the *WHT*, dithered between the four quadrants, were reduced using purpose-built scripts that make use of IRAF tasks. We performed sky subtraction and again median combined the de-dithered images from each epoch into a separate mosaic. Finally, the images of several epochs were combined into a deeper mosaic.

After the basic bias and flat-field corrections of the optical images, further work was done using IRAF and the STARLINK GAIA package (Draper et al. 2009). The H $\alpha$  narrow-band on- and off-filter images and the reduced *Ks*-band images were first aligned with the *R*-band images in IRAF with the GEOMAP and GEOTRAN tasks, in the IMMATCH package, using several field stars identified in each image. Then the continuum was subtracted. The details of this step are described in Section 3.1. The world coordinate systems of *R*-band images were fitted by identifying several ( $\geq 6$ ) field stars whose coordinates are listed in the USNO-A2.0 catalogue, and performing a coordinate transform using the IRAF tasks CCSETWCS and CCMAP in the IMCOORDS package. Then the coordinate systems were copied to corresponding aligned H $\alpha$  and *Ks*-band images. The rms errors of the fits were consistently less than 0.5 arcsec, with one outlier of 0.6 arcsec and a mean of roughly 0.2 arcsec. Assuming that the errors of the reported SN coordinates have a maximum uncertainty of 1.0 arcsec, we estimate a conservative combined error in the coordinates to be of the order of 1 arcsec, comparable to the median seeing in our data. Images of two galaxies, one with high and one with low inclination, observed with typical seeing, are shown in Fig. 2. The NUV data were pre-reduced and the coordinate systems of the images fitted by the *GALEX* pipeline.

For each image in each band, background was subtracted; for H $\alpha$  this was done by the reduction script (see below). For the reduced *R*-band, *Ks*-band and NUV images, background was removed by manually measuring the mean background values in the images and subtracting them.

#### 3.1 Continuum subtraction

In order to study the H $\alpha$  emission of the galaxies, the continuum contribution to the flux in the narrow-band H $\alpha$  images was removed. This was done with the ISIS 2.2 package using the Optimal Image Subtraction (OIS) method presented by Alard & Lupton (1998) and Alard (2000). In order to subtract the continuum accurately, point spread function matching between the on and off images was performed by deriving a space-varying (when needed) convolution kernel. For the kernel derivation, stamps containing a star and some background were identified, including roughly 10 stars (if possible)

<sup>2</sup> <http://galex.stsci.edu/GR6/default.aspx>

**Table 1.** A list of our sample galaxies. ‘Telescope’ given in the form optical/NIR, if both were not observed at the NOT. Seeing FWHM is also given in the form optical/NIR. RA, Dec., distance,  $L_{\text{FIR}}$  from Sanders et al. (2003);  $R_{25}$  and  $i$  from HyperLeda or NED. The  $R_{25}$ ,  $i$  and CCSNe values for galaxy pairs are given for the respective components.

Galaxy	RA (J2000)	Dec. (J2000)	Telescope	FWHM (arcsec)	$D$ (Mpc)	$\lg(L_{\text{FIR}})$ ( $L_{\odot}$ )	$R_{25}$ (arcsec)	$i$ ( $^{\circ}$ )	CCSNe
NGC 157	00 34 46.0	−08 23 53	NOT	1.2/0.8	21.92	10.40	111	61.8	1
UGC 556	00 54 49.9	+29 14 42	NOT	0.9/0.7	60.71	10.73	28	60.9	1
NGC 317B	00 57 40.9	+43 47 37	NOT	1.1/0.6	70.3	11.01	29	65.5	1
NGC 772	01 59 19.5	+19 00 23	NOT	1.7/0.9	28.71	10.37	137	59.6	2
NGC 838	02 09 38.8	−10 08 46	NOT	1.0/0.9	50.13	10.84	40	49.8	1
NGC 922	02 25 04.2	−24 47 21	NOT	0.9/1.0	40.57	10.34	63	33.4	2
NGC 1084	02 45 59.7	−07 34 41	NOT	0.8/0.8	18.61	10.42	102	49.9	3 <sup>a</sup>
NGC 1097	02 46 18.7	−30 16 29	NOT	1.2/0.7	16.8	10.59	314	55.0	3
NGC 1614	04 34 00.1	−08 34 46	NOT	0.9/0.7	62.61	11.43	38	41.8	1
NGC 1961	05 42 03.9	+69 22 33	NOT	0.9/0.8	55.27	10.93	131	47.0	1
NGC 2146	06 18 39.8	+78 21 25	INT/WHT	1.3/0.8	16.47	10.93	161	37.4	1
ESO 492-G02	07 11 40.7	−26 42 19	NOT	1.4/0.6	36.22	10.42	63	48.8	1
UGC 3829	07 23 43.1	+33 26 32	NOT	1.1/0.8	56.37	10.67	31	40.5	1
NGC 2276	07 27 17.8	+85 45 16	NOT	0.9/1.0	35.83	10.68	67	39.8	2
NGC 2415	07 36 56.0	+35 14 31	NOT	0.9/0.9	53.41	10.76	25	0.0	2
NGC 2782	09 14 05.7	+40 06 47	NOT	1.1/0.5	39.51	10.51	97	45.2	1
NGC 2993	09 45 47.3	−14 21 00	NOT	0.9/0.9	34.69	10.55	40	35.8	1
IC 2522	09 55 07.3	−33 08 04	NOT	1.2/1.0	41.16	10.57	69	41.9	2
M82	09 55 53.1	+69 40 41	KP	1.0/1.2	3.63	10.61	329	76.9	2
NGC 3095	10 00 06.2	−31 33 15	NOT	1.1/0.9	36.86	10.46	109	62.1	2
NGC 3094	10 01 25.5	+15 46 15	NOT/WHT	1.3/1.3	37.04	10.50	41	46.2	1
NGC 3079	10 01 57.9	+55 40 51	NOT	0.7/0.7	18.19	10.65	244	90.0	1
NGC 3147	10 16 55.4	+73 23 54	NOT	0.9/0.6	41.41	10.78	122	31.2	1
NGC 3310	10 38 46.2	+53 30 08	NOT/WHT	0.9/1.6	19.81	10.45	57	16.1	1
NGC 3504	11 03 11.1	+27 58 22	NOT/WHT	2.5/1.2	27.07	10.56	74	26.1	2
M66	11 20 14.9	+12 59 30	KP/NOT	1.2/0.4	10.04	10.24	307	67.5	2
NGC 3655	11 22 53.5	+16 35 28	NOT	0.7/0.9	26.42	10.23	45	47.1	1
NGC 3672	11 25 01.6	−09 47 34	NOT	1.5/0.7	27.70	10.37	87	56.2	1
NGC 3683	11 27 30.6	+56 52 44	NOT	0.8/0.8	29.06	10.50	52	68.8	1
NGC 3690/IC 694	11 28 30.4	+58 34 10	NOT/WHT	1.3/0.6	47.74	11.74	72/35	43.6/52.4	3/4
NGC 4027	11 59 28.8	−19 15 45	NOT	0.9/0.6	22.84	10.26	106	42.3	1
NGC 4030	12 00 23.8	−01 06 03	NOT	0.9/0.6	24.50	10.56	114	47.1	1
NGC 4038/9	12 01 55.1	−18 52 43	NOT/WHT	1.7/1.5	21.54	10.73	161/93	51.9/71.2	1/0
NGC 4041	12 02 12.2	+62 08 14	NOT	1.0/0.7	22.78	10.31	77	22.0	1
M61	12 21 55.4	+04 28 24	NOT	1.8/0.7	15.29	10.37	208	18.1	3
NGC 4433	12 27 37.5	−08 16 35	NOT	0.7/0.6	41.68	10.76	60	79.6	1
NGC 4527	12 34 09.9	+02 39 04	NOT	1.8/0.6	15.29	10.29	189	81.2	1
NGC 4567/8	12 36 33.7	+11 14 32	NOT	1.5/0.7	15.29	10.20	83/128	39.4/67.5	0/2
NGC 5020	13 12 39.1	+12 36 07	NOT	0.9/0.9	51.45	10.60	81	27.0	1
NGC 5078	13 19 50.0	−27 24 37	NOT	1.3/0.9	26.32	10.44	77	90.0	1
M51	13 29 52.7	+47 11 43	KP/NOT	1.3/0.5	8.63	10.31	414	32.6	3
UGC 8739	13 49 15.0	+35 15 17	NOT	0.9/0.6	74.18	11.03	57	87.5	1
NGC 5371	13 55 39.1	+40 27 34	NOT	1.2/0.6	41.06	10.57	119	54.0	1
NGC 5394/5	13 58 36.0	+37 25 58	NOT	0.7/0.6	53.40	10.89	52/75	70.8/66.1	0/1
NGC 5433	14 02 37.4	+32 30 27	NOT	1.2/0.7	65.30	10.83	45	90.0	1
NGC 5597	14 24 26.5	−16 45 43	NOT/WHT	0.6/0.9	36.68	10.46	60	40.0	1
NGC 5775	14 53 58.0	+03 32 32	NOT	1.0/0.6	26.34	10.68	111	83.2	1
NGC 6000	15 49 49.4	−29 23 11	NOT/WHT	5.9/1.3	28.90	10.83	57	30.7	2
NGC 6574	18 11 51.0	+14 58 53	NOT	1.4/0.6	35.94	10.66	48	41.5	1
NGC 6643	18 19 47.4	+74 34 09	NOT	1.0/0.6	21.85	10.26	99	62.7	2
NGC 6745	19 01 41.5	+40 44 46	NOT	1.3/0.9	64.81	10.85	29	63.9	1
NGC 6951	20 37 13.9	+66 06 20	NOT	0.8/0.9	23.99	10.46	95	50.8	1
NGC 7479	23 04 57.7	+12 19 29	NOT/WHT	1.3/1.0	32.36	10.58	109	43.0	2
NGC 7678	23 28 27.0	+22 25 09	NOT	1.0/0.7	46.49	10.61	60	43.7	2
NGC 7714	23 36 14.2	+02 09 17	NOT/WHT	1.0/1.4	38.16	10.53	66	45.1	2
NGC 7753	23 47 01.3	+29 28 11	NOT	1.4/0.6	67.46	10.84	60	82.1	1
NGC 7771	23 51 24.7	+20 06 39	NOT	0.8/0.8	57.11	11.23	75	66.7	1

<sup>a</sup>SN 2012ec located in NGC 1084 was still visible when the galaxy was observed, and thus could not be included in this study.

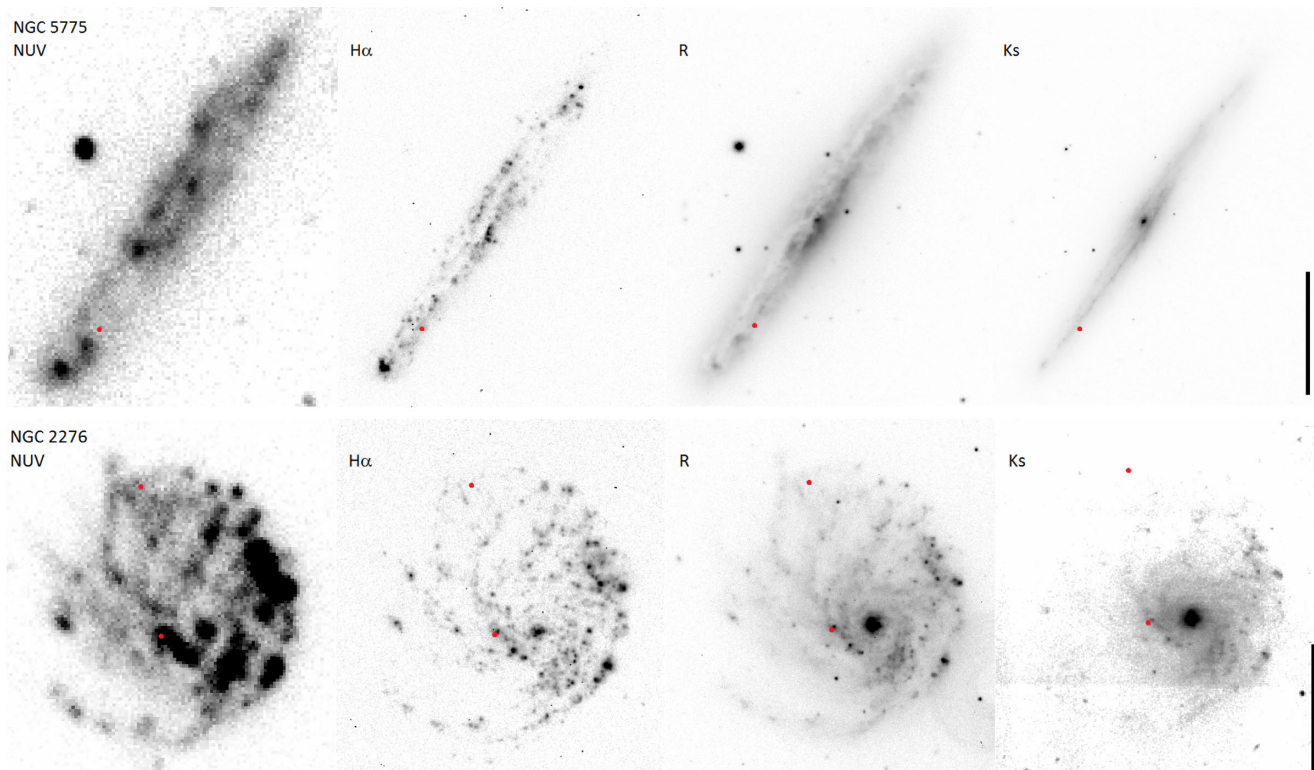


**Figure 2.** The data sets of a high- and low-inclination galaxy with typical seeing; NGC 5775 (upper row) and NGC 2276 (lower row). The black line on the right corresponds to one arcminute, and thus roughly 8 kpc in the NGC 5775 images and 10 kpc in the NGC 2276 images. SN positions are marked with red dots.

of varying brightness as evenly distributed around the galaxy as possible. For each image pair, a few different sets of options – mainly stamp size and the degree of spatial variation – were tested and the best resulting subtracted image (with the most thorough removal of field stars) was chosen. The pixels in the subtracted image were binned by  $2 \times 2$  to improve the signal-to-noise ratio.

Our use of this subtraction method contains the intrinsic assumption that the spectral slope (in this case, in the red region) of the selected stars is, on average, similar to that of the target galaxy’s stellar population. Despite selecting multiple stars of varying brightness, this may not be entirely true because the image is magnitude-limited and thus a selected stamp star has a higher probability to be bright than if its spectral class was completely random. This should be somewhat compensated for by avoiding the very brightest stars in the fields, which has been done here.

Although the methods employed here do not require flux calibration, we have tested the reliability of the subtraction by calibrating the  $H\alpha$  fluxes of three galaxies – NGC 3310, NGC 3504 and NGC 7714 – and checking the values against those reported in the NASA/IPAC Extragalactic Database (NED).<sup>3</sup> All three values match within 10 per cent. For the flux calibration of these  $H\alpha$  images, we used the Isaac Newton Group (ING) list of spectrophotometric standards.<sup>4</sup> The spectra obtained from the ING website were integrated over the response functions of the NOT filters<sup>5</sup> us-

ing the IRAF task SBANDS, in the ONEDSPEC package, to obtain a ‘real’ flux value. This was compared to the photometric flux of our standards, measured with STARLINK GAIA, to obtain a calibration factor, taking into account also the airmass differences between the target and standard images, and the rebinning.

## 4 ANALYSIS METHODS

### 4.1 Pixel statistics

The first statistical method we used was correlating the spatial distribution of SNe with the host galaxy emission using pixel statistics. We analysed the sample using the method presented in James & Anderson (2006), designed to test quantitatively whether SNe of different types follow the  $H\alpha + [N II]$  line emission. This method has already been shown to be robust, and its usage allows comparing our results with previous studies. James & Anderson (2006) used a statistical indicator they named the normalized cumulative rank pixel value function (NCRPVF or NCR for short; we adopt the latter abbreviation) to study the sites of a sample of SNe in  $H\alpha$ . Briefly put, the NCR value of a SN tells the fraction of the host galaxy emission that originates in regions fainter than the pixel at the SN location (for example, an NCR value of 0.1 means 10 per cent of the galaxy flux comes from fainter pixels and 90 per cent from brighter ones). Thus, this value measures the correlation between SNe and the host galaxy emission. In the case of  $H\alpha$  narrow-band images, it measures the correlation between SNe and  $H II$  regions (and therefore young massive stars). The NCR distributions of different CCSN types can then be compared.

The  $H\alpha$  images were trimmed to include the target galaxy and as little background sky as possible, the point where the pixel counts

<sup>3</sup> <http://ned.ipac.caltech.edu/>. NED is operated by the Jet Propulsion Laboratory, California Institute of Technology, under contract with the National Aeronautics and Space Administration.

<sup>4</sup> <http://www.ing.iac.es/Astronomy/observing/manuals/>

<sup>5</sup> <http://www.not.iac.es/instruments/filters/filters.php>

reach the background value was chosen as the edge. This usually meant an image of a few hundred  $\times$  a few hundred pixels, corresponding to  $1\text{--}4 \times 1\text{--}4$  arcmin depending on apparent galaxy size. The pixels of each image were sorted in order of increasing pixel value, giving a sequence from the lowest value (negative) background pixels to the brightest pixels of  $\text{H}\alpha$  emitting regions. Alongside this sequence the corresponding cumulative distribution was formed, each pixel's respective value obtained by summing the pixel counts in the sequence up to the pixel in question. The cumulative sequence ends in the total  $\text{H}\alpha + [\text{N II}]$  flux of the galaxy. This cumulative rank sequence was then divided by the total line emission flux, and the initial negative NCR values were set to zero, giving a normalized cumulative rank pixel value function running from 0 to 1. The formula for the NCR of a pixel can therefore be expressed as

$$\text{NCR}_n = \sum_{i=1}^n P_i / \sum_{j=1}^m P_j, \quad \text{when } \sum_{i=1}^n P_i > 0 \quad (1)$$

$$\text{NCR}_n = 0, \quad \text{when } \sum_{i=1}^n P_i \leq 0 \quad (2)$$

where  $n$  is the rank of the pixel whose NCR we want to find within the ascending sequence,  $P_i$  is the value of a pixel with rank  $i$ , and  $m$  is the total number of pixels. For an illustrative example of the NCR function, see fig. 6 in James & Anderson (2006). In our images, the sequence typically contains roughly  $10^5$  entries. Finally, based on the coordinates of each SN, the pixel containing the SN was found in the image and assigned an NCR value.

Before replacing the initial negative values, the NCR reaches a minimum where individual pixel values reach zero. Since the background sky contains roughly equal numbers of positive and negative pixels after subtraction, and, assuming the subtraction has been done accurately, the average value of these pixels is zero, the NCR reaches zero at the point where the sky ends and the emission regions begin, with a value of 1 representing the core of the very brightest  $\text{H II}$  region or the galactic nucleus. Thus every background pixel has an NCR value of zero in the final sequence, and the choice of how one trims the image has little effect on the result. Since the majority of pixels in  $\text{H}\alpha$  images are considered background, a population that is randomly scattered throughout the host galaxies tends to low NCR values. One closely associated with the very cores of  $\text{H II}$  regions would, on the other hand, have high NCR values, while a population accurately following the underlying emission would have a mean value of 0.5 and a uniform NCR distribution (i.e. a distribution where each NCR value has the same probability).

The same steps were repeated for the  $R$ - and  $Ks$ -band and NUV images to study the correlations between SNe and galaxy light at those wavelengths as well.

#### 4.2 Radial distribution of CCSNe

Another statistical method we employed was to study the radial distribution of the SNe relative to the flux of the host galaxy.

We determined the fraction of  $\text{H}\alpha + [\text{N II}]$  emission flux, hereafter called  $Fr(\text{H}\alpha)$ , as in Habergham et al. (2010), inside an aperture centred on the  $Ks$ -band core of the host galaxy. The aperture was chosen in such a way that the location of the SN in question lies on its outer edge. The flux inside this aperture was then divided by the total  $\text{H}\alpha + [\text{N II}]$  flux of the galaxy. Because of the often irregular shape of our galaxies, we used circular apertures instead of the elliptical ones used by e.g. James & Anderson (2006) to compensate for

inclination effects. Circular apertures were used for all the galaxies in our sample for the purpose of consistency. These measurements were repeated for the  $R$ - and  $Ks$ -band and NUV images. An  $Fr$  value of 0 would mean that the SN in question has exploded precisely at the core of the galaxy, while a value of 1 means an outlying SN at the very edge of the galaxy (or even outside its visible edge).

There are some issues with the radial distribution analysis. First, it is not trivial to define the ‘total flux’ of the galaxy. In this case, we have tried increasing the aperture size until the flux (minus that in the sky annulus) reaches a plateau. Secondly, in some cases it can be difficult to objectively determine where one component of a multiple galaxy system ends and another begins. Anderson et al. (2011) attempted to avoid the issue by using the centre of the Arp 299 system instead of the cores of individual components, and measuring the flux inside the aperture relative to the whole system flux. We, however, are not sure this kind of method produces truly meaningful results. Another method they used was centring the apertures on the A and B1 cores, as we did, but comparing the aperture flux to the total flux of the system. While this method can be used to study the *relative*  $Fr$  values in the system (which was the aim of their study), here we cannot obtain results for a sample of galaxies this way. In the case of close galaxy pairs in this study (NGC 3690/IC694, NGC 4038/9 and NGC 4567/8), we used the point of lowest flux between the galaxies as the separating point. The fluxes for both components were measured separately (which produces an underestimated value). The ratio of the measured component fluxes was then used to determine how large a fraction of the total flux of the whole system belongs to which component and the final fluxes of the components calculated from this.

#### 4.3 Surface density profile of CCSNe

Hakobyan et al. (2009) derived a scale length for the surface density of SNe in spiral galaxies using 224 SNe within 204 host galaxies. They used a radial distance, corrected for projection effects and normalized to  $R_{25}$ , the isophotal radius for the blue-band surface brightness of  $25 \text{ mag arcsec}^{-2}$ , to determine a normalized surface density in each distance bin, and fitted an exponential function of the form  $\Sigma^{\text{SN}}(\tilde{r}) = \Sigma_0^{\text{SN}} \exp(-\tilde{r}/\tilde{h}_{\text{SN}})$ . Here  $\tilde{r}$  is the distance normalized to  $R_{25}$  and  $\tilde{h}_{\text{SN}}$  is the scale length of the surface density, also normalized to  $R_{25}$ . Herrero-Illana, Pérez-Torres & Alberdi (2012) applied the same method to VLBI-observed SN remnants and radio SNe in a starburst galaxy, a LIRG and an ULIRG. We similarly determine a normalized surface density distribution for our sample of CCSNe.

We calculated the de-projected distance of each SN to the centre of its host galaxy according to equations (1) and (2) in Hakobyan et al. (2009):

$$U = \Delta\alpha \sin\text{PA} + \Delta\delta \cos\text{PA}, \quad V = \Delta\alpha \cos\text{PA} - \Delta\delta \sin\text{PA} \quad (3)$$

$$R_{\text{SN}}^2 = U^2 + \left(\frac{V}{\cos i}\right)^2 \quad (4)$$

where  $U$  and  $V$  are the coordinates of the SN in the host galaxy's coordinate system, PA is the major axis position angle,  $\Delta\alpha$  and  $\Delta\delta$  are the coordinate differences between the SN and the galaxy core,  $i$  is the galaxy inclination and  $R_{\text{SN}}$  is the true SN-core distance. However, during our analysis, it became clear that as the inclination of the host galaxy approaches  $90^\circ$ , the calculated distance becomes too large to be trustworthy. Thus, galaxies with inclination  $>70^\circ$  were excluded from this study, leaving us with 77 SNe in 49 galaxies.

The de-projected distances were normalized to the  $R_{25}$  of the host galaxy. The coordinates of the cores were determined from the  $Ks$ -band images. The  $R_{25}$  distances, position angles of the major axes of the galaxies and inclinations of the galactic discs were obtained from the HyperLeda data base<sup>6</sup> (Paturel et al. 2003) if available. If the HyperLeda data base did not have the information for a particular galaxy, we used NED instead. We then divided the normalized distance distribution into quartile bins. The surface density in each bin was determined by dividing the number of SNe in the bin by the area of a concentric ring (normalized to  $R_{25}^2$ ), with the limits of the bin as the inner and outer edges of the ring, around the nucleus. The unit of surface density is thus  $R_{25}^{-2}$ .

We fitted two different disc profiles, an exponential disc of the form  $\Sigma^{SN}(\tilde{r}) = \Sigma_0^{SN} \exp(-\tilde{r}/\tilde{h}_{SN})$  and a disc with power-law surface density profile  $\Sigma^{SN}(\tilde{r}) = \Sigma_0^{SN} \tilde{r}^{-\gamma}$ , to the data. The first case assumes that the SN distribution follows the radial surface brightness distribution in spiral discs (Freeman 1970); while the second has been used to probe profiles predicted by numerical simulations (Wada & Norman 2002). Since our sample sizes in each bin are relatively small, we performed a Monte Carlo (MC) simulation to obtain more reliable values for the fit parameters, similarly to Herrero-Illana et al. (2012). We generated 10 000 mock samples whose surface density values in each bin are uniformly distributed within the Poissonian uncertainty of each data point. We then fitted the exponential and power-law functions to each of these samples to obtain 10 000 sets of parameters. We then used the median values of the parameters  $\gamma$  and  $\tilde{h}_{SN}$  from the MC distributions. The uncertainty in these values was set at the 90 per cent confidence level.

## 5 RESULTS

### 5.1 Pixel statistics

The NCR values based on the  $H\alpha + [N II]$  line,  $R$  and  $Ks$  band and NUV light are listed in Table 2, along with the results for the radial distribution (see below), for the 86 CCSNe. We have grouped our CCSNe into two subsamples, those of Type Ibc/I Ib, thought to have stripped envelope progenitors, and the remaining Type II SNe. In Table 3 we present the mean NCR values of all subsamples, along with the standard errors of the mean and the number of SNe in the different groups. In this table and others, the Ibc subsample also includes the SNe classified as Ib/c, which are not included in the Ib or Ic groupings. The distributions of SNe are presented on the left-hand side of Fig. 3 as cumulative distribution functions (CDFs). The mean NCR( $H\alpha$ ) value ( $\pm$  SEM) of Type Ibc/I Ib SNe is statistically significantly larger ( $0.475 \pm 0.052$ ) than for Type II ( $0.268 \pm 0.038$ ). Further separating the Type Ibc sample into Ib and Ic subsamples, we find a mean NCR of  $0.607 \pm 0.068$  for Ic as opposed to  $0.290 \pm 0.074$  for Ib, implying Type Ic having a stronger association with  $H II$  regions than Ib – and that, within the error limits, the correlations for Types II and Ib are roughly equal. In the  $R$  band, the difference between the average values for the two types is somewhat less ( $0.619 \pm 0.041$  for Type Ibc/I Ib versus  $0.516 \pm 0.041$  for Type II). The NCR( $Ks$ ) values are closer to the ones from  $H\alpha$  images, with a mean of  $0.499 \pm 0.041$  for Type Ibc/I Ib and  $0.394 \pm 0.043$  for Type II. Finally, in the NUV, the difference between the two types is just within the error:  $0.614 \pm 0.052$  for Type Ibc/I Ib and  $0.525 \pm 0.047$  for Type II. For subtypes of Type I,

we get  $0.482 \pm 0.112$  for Type Ib and  $0.666 \pm 0.072$  for Ic; the difference is just barely larger than the error. This indicates Type Ib events more closely follow the host galaxy's NUV light distribution, while Type Ic SNe preferably occur in the brighter regions.

A12 obtained a mean NCR( $H\alpha$ ) value of  $0.254 \pm 0.023$  for Type II SNe, which is consistent with our value for Type II. For Type Ibc, they obtained a mean value of  $0.390 \pm 0.031$ , which is significantly less than our corresponding value,  $0.500 \pm 0.055$ .

We used the Kolmogorov–Smirnov (KS) test to compare our distributions to a hypothetical flat (i.e. uniform) distribution. All results for the KS tests are listed in Table 4. Since the NCR tells how large a fraction of the galaxy's flux comes from pixels fainter than the SN's location, a similar fraction of CCSNe should also explode in fainter pixels. Therefore, if the SNe accurately follow the  $H\alpha + [N II]$  line emission, the distribution of NCR values should be flat, with a mean of 0.5. Thus, this comparison tells us how strongly each sub-sample, or the whole population of CCSNe, is correlated with the star-forming regions. We found that the distribution of the NCR values of Type Ibc/I Ib SNe is formally consistent with a flat distribution, and the mean NCR value is indeed consistent with 0.5 within the error. The NCRs of Type II SNe, on the other hand, do differ from a flat distribution, with the probability of the distributions being the same being under 0.1 per cent. Thus, Type Ibc/I Ib SNe do seem to follow the  $H\alpha + [N II]$  line emission rather well, while Type II SNe do not.

We repeated this test for the NCR values from the other bands, and found that, in the  $R$  band, the Ibc/I Ib sample significantly differs from a flat distribution while Type II does not. However, the Type Ib sample seems to trace the galaxy light as well. In the  $Ks$ -band, the results are similar to  $H\alpha$ , with a statistically significant difference from a flat distribution for Type II but not for Type Ibc/I Ib, but the test cannot detect differences between Types Ib and Ic. In the NUV, only the Ic sample significantly differs from a flat distribution. With a mean value very close to 0.5, however, Type II follows the galaxy emission more accurately than Types Ibc/I Ib.

Furthermore, we performed two-sample KS tests to compare the distributions of the different types. The difference between the distributions of Types Ibc/I Ib and II is significant in  $H\alpha$  and in the  $Ks$  band – and subtypes Ib and Ic also show a significant difference in  $H\alpha$ . This agrees quite well with the differences in mean NCR values. Further two-sample tests were performed between the  $H\alpha$  and NUV values, to see if the distributions match regarding recent and on-going star formation. The only significant difference here is for Type II.

### 5.2 Radial distribution of CCSNe

The  $Fr$  values for all wavelengths are listed in Table 2, and their cumulative distributions are presented on the right-hand side of Fig. 3. The mean values and standard errors of the mean are listed in Table 5. The radial distributions of SNe of different types do not have a difference as big as the NCR values: the mean  $Fr(H\alpha)$  for Type Ibc/I Ib is  $0.488 \pm 0.044$ , while for Type II SNe it is  $0.502 \pm 0.046$ . For subtypes Ib and Ic the values are  $0.575 \pm 0.088$  and  $0.451 \pm 0.059$ , respectively. In the  $R$  band, the values are consistent with those in  $H\alpha$  within the errors:  $0.438 \pm 0.043$  for Ibc/I Ib,  $0.474 \pm 0.087$  for Ib,  $0.443 \pm 0.059$  for Ic and  $0.469 \pm 0.041$  for Type II. In the  $Ks$  band we see a difference to the  $H\alpha$  and  $R$  band, with a mean value of  $0.561 \pm 0.044$  for Types Ibc/I Ib and  $0.607 \pm 0.042$  for Type II; while the NUV values are close to the ones from  $R$  band,  $0.426 \pm 0.052$  for Ibc/I Ib and  $0.453 \pm 0.047$  for Type II.

<sup>6</sup> <http://leda.univ-lyon1.fr/>

**Table 2.** The main results for the CCSN sample from H $\alpha$ , R and Ks band and NUV images.

SN	Type	Host galaxy	NCR(H $\alpha$ )	NCR(R)	NCR(Ks)	NCR(NUV)	Fr(H $\alpha$ )	Fr(R)	Fr(Ks)	Fr(NUV)
2012es	I Ib	NGC 5597	0.125	0.538	0.375	0.666	0.640	0.463	0.621	0.434
2011dh	I Ib	M51	0.028	0.274	0.053	0.569	0.659	0.798	0.464	0.757
2010gk	I Ic	NGC 5433	0.818	0.833	0.622	0.934	0.327	0.614	0.576	0.168
2010bk	II P	NGC 4433	0.589	0.711	0.840	0.761	0.101	0.058	0.160	0.036
2010as	Ib/c	NGC 6000	0.678	0.815	0.686	—	0.238	0.160	0.336	—
2010P	Ib/IIb	NGC 3690	0.354	0.563	0.488	0.537	0.789	0.504	0.609	0.487
2010O	Ib	IC 694	0.497	0.864	0.603	0.455	0.277	0.123	0.286	0.103
2009jf	Ib	NGC 7479	0.532	0.282	0.152	0.880	0.569	0.675	0.796	0.524
2009hd	II	M66	0.776	0.619	0.579	0.685	0.306	0.413	0.569	0.362
2009ga	II P	NGC 7678	0.210	0.646	0.484	0.426	0.712	0.589	0.719	0.605
2009em	Ic	NGC 157	0.457	0.576	0.390	0.671	0.283	0.350	0.576	0.321
2009H	II	NGC 1084	0.354	0.385	0.294	0.324	0.585	0.593	0.795	0.536
2008iz	II	M82	0.337	0.793	0.936	0.915	0.084	0.014	0.126	0.007
2008in	II P	M61	0	0.188	0.011	0.160	0.937	0.850	0.932	0.810
2008ij	II	NGC 6643	0.479	0.421	0.225	—	0.383	0.322	0.696	—
2008ho	II P	NGC 922	0.532	0.445	0.117	0.668	0.928	0.892	0.922	0.881
2008gz	II	NGC 3672	0.232	0.877	0.649	0.913	0.109	0.162	0.198	0.057
2008eb	Ic	NGC 6574	0.273	0.410	0.318	0.154	0.767	0.594	0.631	0.645
2008co	—	IC 2522	0.693	0.915	0.879	0.705	0.028	0.057	0.094	0.043
2008br	II	IC 2522	0	0.640	0.285	0.717	0.060	0.153	0.237	0.206
2008bp	II P	NGC 3095	0	0.288	0	0.279	0.221	0.387	0.583	0.584
2008bo	Ib	NGC 6643	0	0.637	0.530	—	0.657	0.513	0.982	—
2007fo	Ib	NGC 7714	0.226	0.529	0.556	0.304	0.702	0.556	0.454	0.624
2007ch	II	NGC 6000	0.146	0.394	0.220	—	0.752	0.577	0.798	—
2007aa	II P	NGC 4030	0.157	0.056	0	0.318	0.963	0.968	0.985	0.953
2006ov	II P	M61	0.165	0.771	0.647	0.890	0.387	0.459	0.571	0.358
2006gi	Ib	NGC 3147	0	0	0.018	0.035	1	1	1	0.990
2006A	—	NGC 7753	0.139	0.707	0.754	0.549	0.060	0.238	0.186	0.072
2005kh	II	NGC 3094	0	0	0.02	0.016	1	1	1	0.889
2005lr	Ic	ESO 492-G02	0.246	0.493	0.321	—	0.759	0.427	0.802	—
2005eb	II	UGC 556	0.680	0.611	0.239	0.800	0.744	0.535	0.772	0.360
2005dl	II	NGC 2276	0.768	0.849	0.714	0.863	0.070	0.105	0.391	0.145
2005cs	II P	M51	0.505	0.741	0.574	0.896	0.224	0.312	0.232	0.204
2005V	Ib/c	NGC 2146	0.848	0.934	0.695	0.917	0.072	0.023	0.179	0.004
2005U	IIb	IC 694	0.622	0.849	0.613	0.848	0.341	0.173	0.338	0.160
2005H	II	NGC 838	0.566	0.685	0.560	0.785	0.306	0.188	0.280	0.105
2004gt	Ic	NGC 4038	0.863	0.974	0.925	0.996	0.844	0.655	0.812	0.725
2004gn	Ic	NGC 4527	0.663	0.633	0.443	0	0.350	0.599	0.925	0.404
2004ej	II	NGC 3095	0	0.142	0.073	0.289	0.130	0.271	0.452	0.368
2004cc	Ic	NGC 4568	0.714	0.912	0.841	0.564	0.190	0.165	0.262	0.064
2004bf	Ic	UGC 8739	0.874	0.885	0.393	0.787	0.492	0.750	0.873	0.559
2004am	II P	M82	0.547	0.965	0.884	0.606	0.582	0.240	0.564	0.098
2004C	Ic	NGC 3683	0.950	0.618	0.626	0.676	0.707	0.670	0.896	0.508
2003iq	II	NGC 772	0	0.402	0.160	0.558	0.374	0.534	0.885	0.338
2003hl	II	NGC 772	0.262	0.689	0.414	0.773	0.198	0.340	0.657	0.174
2003hg	II	NGC 7771	0.246	0.659	0.673	0.556	0.453	0.215	0.455	0.351
2003ao	II P	NGC 2993	0.037	0.487	0.374	0.531	0.531	0.319	0.358	0.637
2003B	II P	NGC 1097	0	0.027	0	0.064	1	0.969	1	0.812
2002ji	Ib/c	NGC 3655	0.131	0.250	0.057	0.360	0.472	0.513	0.692	0.724
2002gw	II	NGC 922	0	0.211	0.204	0.182	0.799	0.825	0.820	0.764
2001is	Ib	NGC 1961	0.333	0.263	0	0.784	0.200	0.281	0.743	0.381
2001ej	Ib	UGC 3829	0.163	0.585	0.531	—	0.851	0.445	0.317	—
2001ci	Ic	NGC 3079	0.221	0.725	0.671	0.475	0.242	0.145	0.310	0.093
2001ac	II n	NGC 3504	0	0.153	0.082	0	0.988	0.865	0.875	0.923
2000cr	Ic	NGC 5395	0.925	0.627	0.558	0.829	0.822	0.831	0.719	0.774
2000C	Ic	NGC 2415	0.670	0.392	0.631	0.675	0.399	0.301	0.737	0.720
1999gn	II P	M61	0.581	0.769	0.542	0.873	0.408	0.469	0.580	0.372
1999gl	II	NGC 317B	0.340	0.732	0.609	0.920	0.687	0.145	0.329	0.110
1999eu	II P	NGC 1097	0	0.159	0	0.143	0.994	0.934	1	0.738
1999el	II n	NGC 6951	0	0.646	0.551	0.440	0.251	0.137	0.646	0.179
1999dn	Ib	NGC 7714	0.072	0.416	0.399	0.243	0.759	0.599	0.484	0.686
1999bx	II	NGC 6745	0.268	0.646	0.299	—	0.380	0.462	0.299	—
1999cz	Ic	NGC 5078	0	0.609	0.365	0.811	0.595	0.561	0.776	0.814
1999D	II	NGC 3690	0	0.271	0.134	0.165	1	0.785	0.791	0.978

**Table 2** – *continued*

SN	Type	Host galaxy	NCR(H $\alpha$ )	NCR(R)	NCR(Ks)	NCR(NUV)	Fr(H $\alpha$ )	Fr(R)	Fr(Ks)	Fr(NUV)
1998dl	II P	NGC 1084	0.268	0.375	0.216	0.455	0.559	0.575	0.778	0.512
1998cf	–	NGC 3504	0.915	0.972	0.979	0.925	0.031	0.016	0.028	0.011
1998Y	II	NGC 2415	0.248	0.679	0.567	0.866	0.223	0.178	0.500	0.465
1998T	Ib	IC 694	0.672	0.864	0.658	0.848	0.275	0.139	0.304	0.123
1997dc	Ib	NGC 7678	0.407	0.691	0.602	0.310	0.120	0.127	0.227	0.068
1997bs <sup>a</sup>	IIIn	M66	0.281	0.452	0.336	0.315	0.669	0.538	0.725	0.637
1996W	II	NGC 4027	0.879	0.803	0.707	–	0.767	0.540	0.797	–
1996an	II	NGC 1084	0.268	0.902	0.701	0.955	0.443	0.506	0.710	0.419
1996ae	IIIn	NGC 5775	0.626	0.490	0.328	0.271	0.665	0.782	0.923	0.575
1996D	Ic	NGC 1614	0.326	0.433	0.383	–	0.264	0.065	0.300	–
1994ak	IIIn	NGC 2782	0	0.196	0	0.321	0.831	0.52	1	0.818
1994Y	IIIn	NGC 5371	0	0.614	0.609	0.057	0.149	0.414	0.458	0.181
1994W <sup>b</sup>	IIIn	NGC 4041	0.232	0.432	0.247	0.629	0.302	0.513	0.804	0.340
1994I	Ic	M51	0.643	0.875	0.821	0.934	0.061	0.107	0.060	0.048
1993X	II	NGC 2276	0.007	0.231	0	0.295	0.515	0.619	1	0.957
1993G	II L	IC 694	0	0.212	0.095	0.097	0.823	0.604	0.734	0.634
1992bu	–	NGC 3690	0.227	0.675	0.471	0.538	0.309	0.261	0.434	0.210
1992bd	II	NGC 1097	0.325	0.986	0.979	0.865	0.008	0.003	0.007	0.001
1991N	Ic	NGC 3310	0.890	0.916	0.818	0.996	0.252	0.296	0.379	0.252
1991J	II	NGC 5020	0.711	0.961	0.931	0.927	0.007	0.020	0.060	0.019
1990U	Ic	NGC 7479	0.559	0.496	0.349	0.753	0.601	0.697	0.815	0.554
1990B	Ic	NGC 4568	0.842	0.883	0.815	0.402	0.173	0.152	0.245	0.054

<sup>a</sup>SN 1997bs has been considered an SN ‘impostor’ by Van Dyk et al. (2000), but there is also evidence that this is not the case (Li et al. 2002). Thus we decided to keep it in the sample.

<sup>b</sup>The SN nature of SN 1994W has been questioned (Dessart et al. 2009); however, contrary evidence for alike transients has also been found; see e.g. the discussion of Kankare et al. (2012). Thus we decided to keep it in the sample as well.

**Table 3.** The mean H $\alpha$ , R and Ks band and NUV NCR values of the CCSNe, with comparison values from A12.

SN type	N	NCR(H $\alpha$ )	NCR(H $\alpha$ , A12)	NCR(R)	NCR(Ks)	NCR(NUV)
Ibc/IIb	35	0.475 $\pm$ 0.052	–	0.619 $\pm$ 0.041	0.499 $\pm$ 0.041	0.614 $\pm$ 0.052
II	47	0.268 $\pm$ 0.038	0.254 $\pm$ 0.023	0.516 $\pm$ 0.041	0.394 $\pm$ 0.043	0.525 $\pm$ 0.047
Ibc	31	0.500 $\pm$ 0.055	0.390 $\pm$ 0.031	0.627 $\pm$ 0.044	0.513 $\pm$ 0.044	0.607 $\pm$ 0.059
Ib	10	0.290 $\pm$ 0.074	0.318 $\pm$ 0.045	0.515 $\pm$ 0.088	0.418 $\pm$ 0.084	0.482 $\pm$ 0.112
Ic	18	0.607 $\pm$ 0.068	0.469 $\pm$ 0.040	0.683 $\pm$ 0.046	0.572 $\pm$ 0.049	0.666 $\pm$ 0.072
All	86	0.363 $\pm$ 0.033	–	0.573 $\pm$ 0.029	0.454 $\pm$ 0.031	0.567 $\pm$ 0.034

The differences between the two main types are well within the errors in all bands and thus statistically insignificant. The differences between Ib and Ic samples are small except in H $\alpha$ , but because these samples are rather small, the errors are too large to detect a significant difference there either.

Similarly to the NCR statistics, the distribution of *Fr* is flat if the CCSN distribution accurately traces the galaxy’s emission, with an average value of 0.5 (James & Anderson 2006). The average *Fr*(H $\alpha$ ) values of all our subsamples are indeed close to this value, while in the R band and NUV they are slightly smaller and in the Ks band slightly larger. Similarly to our analysis of NCR values, we performed a KS test to see if the radial distribution matches that of the host galaxy emission. We found that the only statistically significant difference in this analysis is between Type II and a flat distribution in the Ks band, indicating that Type II SNe preferably occur in the outer regions of galaxies, while all other distributions are formally consistent (probability over 10 per cent) with a flat distribution.

Comparing Types I versus II and Ib versus Ic in a two-sample KS test, we found no significant difference between the *Fr* distributions in any band. This result is in agreement with the comparison of the

mean *Fr*(H $\alpha$ ), *Fr*(Ks) and *Fr*(NUV) values of the types. A comparison between the H $\alpha$  and NUV distributions for each type yielded no significant differences.

### 5.3 Surface density profile of CCSNe

The resulting power-law and exponential fits from our MC analysis are plotted in Fig. 4 and the parameters listed in Table 6. We obtained the following values for the parameters of these functions (for details, see Section 4.3):  $\gamma = 1.6 \pm 0.2$ ,  $\tilde{h}_{\text{SN}} = 0.23^{+0.03}_{-0.02}$ . For their sample of 224 SNe, Hakobyan et al. (2009) derived a normalized scale length of  $\tilde{h}_{\text{SN}} = 0.29 \pm 0.01$ , statistically significantly above the value we have obtained. For a Freeman disc, they obtained  $\tilde{h}_{\text{SN}} = 0.32 \pm 0.03$ .

We also compared the Type Ibc/IIb and Type II subsamples’ surface density profiles, obtaining a scale length  $\tilde{h}_{\text{SN}} = 0.19^{+0.03}_{-0.02}$  for Type Ibc/IIb and  $\tilde{h}_{\text{SN}} = 0.29^{+0.06}_{-0.04}$  for Type II, which indicates that Type Ibc/IIb SNe are more centrally concentrated than Type II. This indication is in agreement with previous studies: Hakobyan et al. (2009) obtained scale lengths of  $0.24 \pm 0.03$  for Type Ibc

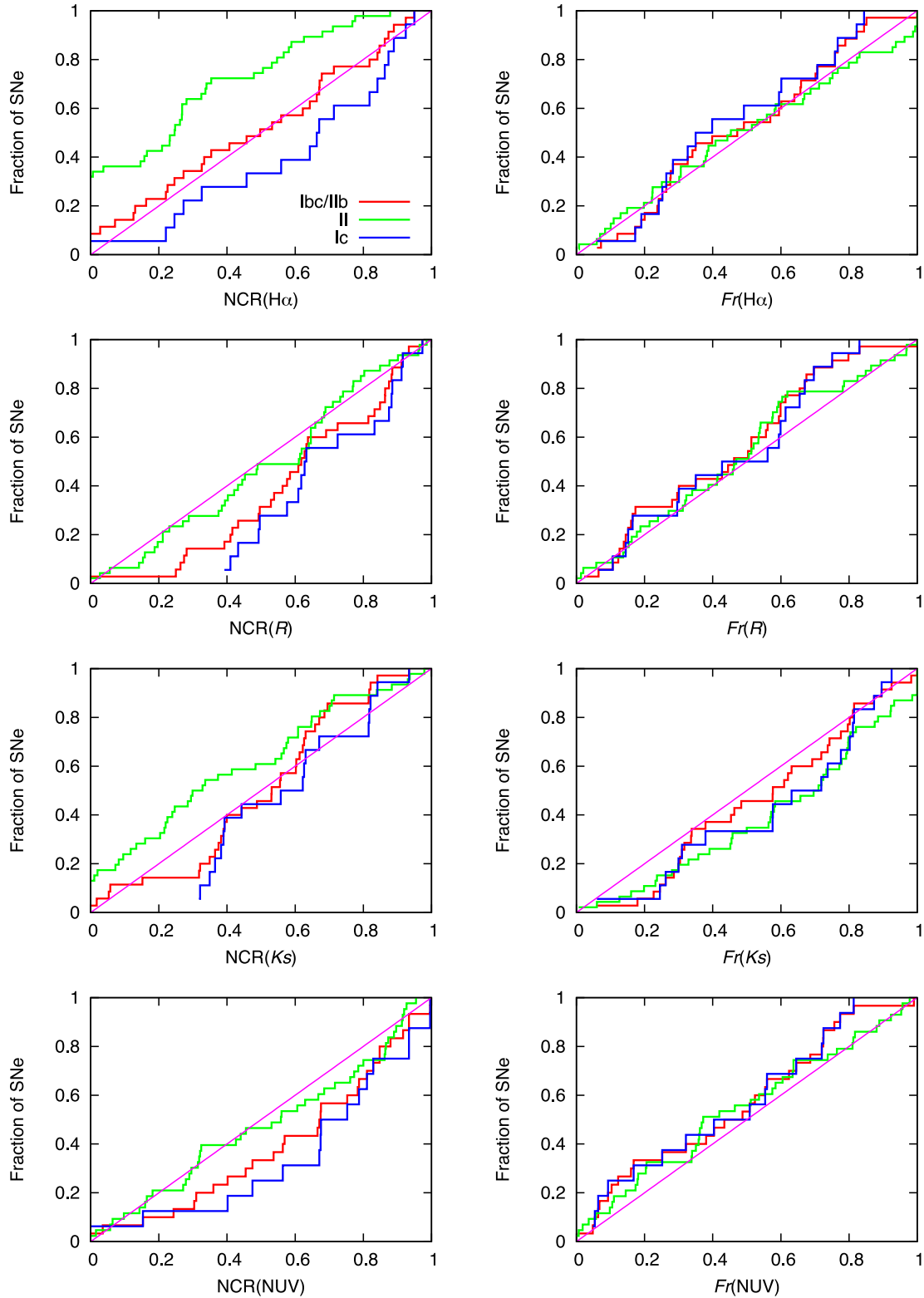


**Figure 3.** The cumulative distributions of NCR (left) and  $Fr$  (right) values for the SNe of different types in different bands. The red lines represent the Type Ibc/IIb subsample, the blue lines just the Type Ic and the green lines the Type II subsample, while the purple diagonal line is the CDF for a flat distribution.

and  $0.31 \pm 0.02$  for Type II. In light of the different scale lengths for Hakobyan's sample and ours, and of the rapidly rising surface density of Types Ibc/IIb in the central region, we obtained  $\tilde{h}_{\text{SN}} = 0.24^{+0.05}_{-0.04}$  for Types Ibc/IIb by ignoring the innermost radial distance

bin, which agrees with Hakobyan et al. (2009). The scale lengths for Type II SNe in their sample and ours are consistent within the errors. The slopes of the power-law fits for the subsamples hint at Type Ibc/IIb SN density falling off more rapidly as well, although

**Table 4.** Results of the KS tests between different samples and between the samples and a flat distribution, given as probabilities (per cent) that the compared distributions are the same. When a difference is significant at the 90 percent confidence level, the corresponding value is written in bold.

Distr.	Ibc/Iib versus flat	II versus flat	Ibc/Iib versus II	Ib versus flat	Ib versus II	Ic versus flat	Ic versus II
NCR(H $\alpha$ )	95	<b>&lt; 0.1</b>	<b>2.7</b>	10	97	43	<b>&lt; 1</b>
NCR(R)	<b>5.6</b>	71	20	> 99	99	<b>2.5</b>	11
NCR(Ks)	29	<b>4.7</b>	<b>1.2</b>	15	60	14	<b>&lt; 1</b>
NCR(NUV)	16	81	47	90	93	<b>9.9</b>	23
Fr(H $\alpha$ )	66	94	78	> 99	60	73	81
Fr(R)	15	13	88	63	98	46	69
Fr(Ks)	46	<b>8.2</b>	70	> 99	57	51	91
Fr(NUV)	35	35	84	62	95	59	89

**Table 5.** The mean H $\alpha$ , R and Ks band and NUV Fr values of the CCSNe, with comparison values (marked H12) for the SNe from Habergham et al. (2012) and Stacey Habergham (private communication).

SN type	<i>N</i>	Fr(H $\alpha$ )	Fr(H $\alpha$ , H12)	Fr(R)	Fr(Ks)	Fr(NUV)
Ibc/Iib	35	0.488 $\pm$ 0.044	0.465 $\pm$ 0.024	0.438 $\pm$ 0.043	0.561 $\pm$ 0.046	0.426 $\pm$ 0.052
II	47	0.502 $\pm$ 0.046	0.552 $\pm$ 0.027	0.469 $\pm$ 0.041	0.607 $\pm$ 0.042	0.453 $\pm$ 0.047
Ibc	31	0.472 $\pm$ 0.048	0.456 $\pm$ 0.026	0.433 $\pm$ 0.046	0.570 $\pm$ 0.051	0.420 $\pm$ 0.058
Ib	10	0.575 $\pm$ 0.088	0.524 $\pm$ 0.047	0.474 $\pm$ 0.087	0.578 $\pm$ 0.102	0.437 $\pm$ 0.117
Ic	18	0.451 $\pm$ 0.059	0.431 $\pm$ 0.037	0.443 $\pm$ 0.059	0.594 $\pm$ 0.063	0.419 $\pm$ 0.070
All	86	0.478 $\pm$ 0.032	0.503 $\pm$ 0.018	0.441 $\pm$ 0.029	0.569 $\pm$ 0.031	0.423 $\pm$ 0.034

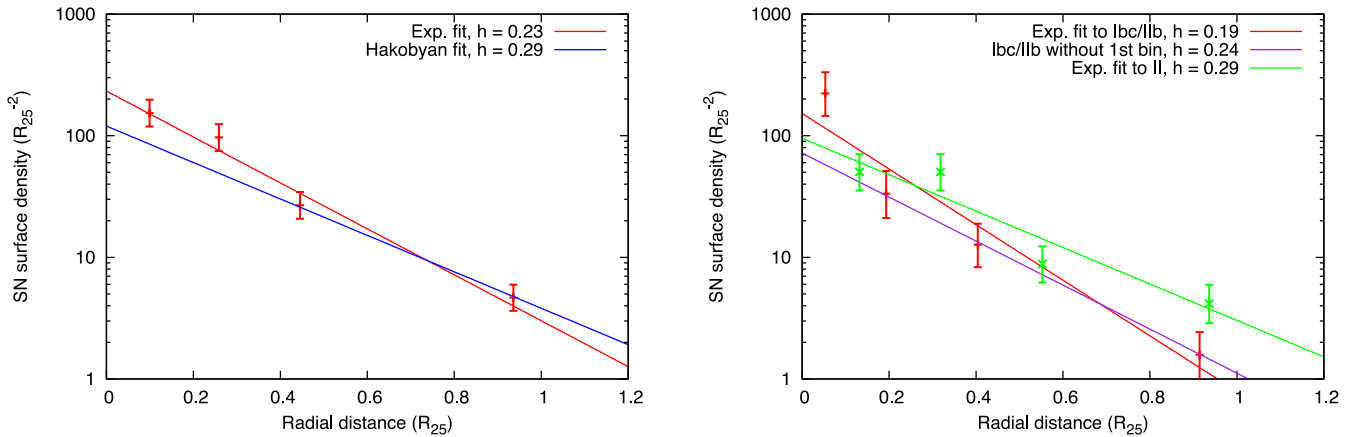


**Figure 4.** The SN surface density values as a function of radial distance (points with error bars) and exponential fits derived from our MC analysis (straight lines). The full sample is on the left and a comparison between subsamples is presented on the right (red for Types Ibc/Iib and green for Type II). The scale length derived by Hakobyan et al. (2009) only fits the outer regions for our sample, while for fitting the full sample a shorter scale length is required. The scale length for Types Ibc/Iib is also shorter than for Type II, although the difference is somewhat mitigated if one ignores the most central radial distance bin.

**Table 6.** The parameters of surface density profiles of CCSNe,  $\tilde{h}_{\text{SN}}$  being the scale length of an exponential function and  $\gamma$  the slope of a power law on a log-log scale.

Sample	$\tilde{h}_{\text{SN}}$	$\gamma$
All CCSNe ( $R_{25}$ )	0.23 $^{+0.03}_{-0.02}$	1.6 $\pm$ 0.2
Hakobyan et al. (2009)	0.29 $\pm$ 0.01	—
Freeman disc	0.32 $\pm$ 0.03	—
Ibc/Iib	0.19 $^{+0.03}_{-0.02}$	1.7 $\pm$ 0.2
Ibc/Iib without 1st bin	0.24 $^{+0.05}_{-0.04}$	—
II	0.29 $^{+0.06}_{-0.04}$	1.4 $^{+0.2}_{-0.3}$
All CCSNe ( $R_{20}$ )	0.34 $^{+0.04}_{-0.03}$	1.6 $\pm$ 0.2
All CCSNe (kpc)	3.7 $\pm$ 0.2	1.8 $^{+0.2}_{-0.1}$

the difference is not statistically significant;  $\gamma(\text{Ibc/Iib}) = 1.7 \pm 0.2$  and  $\gamma(\text{II}) = 1.4^{+0.2}_{-0.3}$ .

In addition, we calculated the mean normalized distances for both subsamples, presented in Table 7. For Type Ibc/Iib, we obtained a mean of  $0.350 \pm 0.055 R_{25}$ , while for Type II it is  $0.476 \pm 0.045$ . Thus, again, the Type Ibc/Iib SNe seem more centrally concentrated than Type II. Furthermore, we converted the corrected angular radial distances into linear distances in parsec. Although the sizes of the galaxies vary, statistically a comparison between the linear distances for each type can be meaningful. We found a mean radial distance of  $5150 \pm 1220$  pc for Type Ibc/Iib and  $6640 \pm 810$  pc for Type II. Again, there is a difference between types, but the error bars are too large to make it statistically significant. The large variations in galaxy sizes make the standard deviation of the linear distance values large as well.

**Table 7.** The mean distances of different CCSN types from the galaxy cores, normalized to  $B$ -band  $R_{25}$  or  $Ks$ -band  $R_{20}$  and also given in parsec. SNe in galaxies with  $i \geq 70^\circ$  have been excluded.

SN type	$N$	$R_{\text{SN}}/R_{25}$	$R_{\text{SN}}/R_{20}$	$R_{\text{SN}}(\text{pc})$
Ibc/IIb	30	$0.350 \pm 0.055$	$0.521 \pm 0.086$	$5150 \pm 1220$
II	43	$0.476 \pm 0.045$	$0.695 \pm 0.074$	$6640 \pm 810$
Ibc	26	$0.367 \pm 0.062$	$0.530 \pm 0.094$	$5460 \pm 1390$
Ib	10	$0.385 \pm 0.119$	$0.724 \pm 0.221$	$7820 \pm 3250$
Ic	13	$0.379 \pm 0.079$	$0.476 \pm 0.101$	$4520 \pm 1110$
All	77	$0.410 \pm 0.034$	$0.608 \pm 0.056$	$5840 \pm 670$

Since most of the galaxies in our sample are dusty, and dust extinction affects the  $B$  band much more strongly than the  $Ks$  band, there was a concern that the  $B$ -band  $R_{25}$  might not offer a valid distance normalization in this case. Thus, we also fitted an exponential function and a power law to distances normalized using the  $K$ -band  $R_{20}$  instead, as measured by 2MASS. While the scale lengths of these functions are not comparable due to the normalization distances being measured at different bands, and the scale length obtained using  $R_{20}$  ( $0.34^{+0.04}_{-0.03}$ ) is not comparable with previous results normalized using  $R_{25}$ , the power laws fitted in both cases are equal. Thus there seems to be no discrepancy.

## 6 DISCUSSION

### 6.1 Possible biases

Comparing our  $\text{NCR}(H\alpha)$  values and those of A08 and A12 (this includes 46 SNe in total; see Fig. 5 for comparison), we see no systematic difference between the two sets. Most of the outlying values seem to be caused by an error in the astrometric calibration of either image. The NCR values for these SNe are 0.281 (0.023 from A08/A12) for SN 1997bs, 0.581 (0.897) for SN 1999gn, 0.925 (0) for SN 2000cr, 0.479 (0.096) for SN 2008ij and 0.776 (0.398) for SN 2009hd. We determined NCR values for the pixels surrounding the SN positions up to a radius of 1 arcsec, and values roughly agreeing with those in A08 and A12 were found among these pixels, suggesting a possibility of small positional errors. For SN 2000cr in particular, the NCR difference is very large, but it is located in a compact bright region. In addition, SN 2005V's value in A08 is

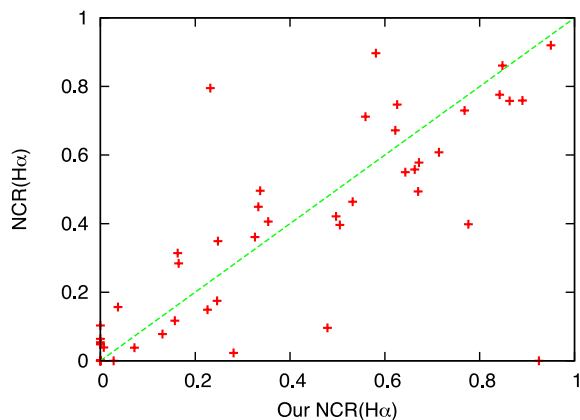


**Figure 5.** A comparison between our  $\text{NCR}(H\alpha)$  values and corresponding values in A08 and A12 for those SNe also included in their study. There is no systematic difference between the two sets of values.

given as 0.000. However, James & Anderson (2006) originally gave it an  $\text{NCR}(H\alpha)$  of 0.861, which is consistent with our value, and we have used this for Fig. 5. The mean  $\text{NCR}(H\alpha)$  of these 46 overlapping SNe is  $0.391 \pm 0.046$  from our values and  $0.367 \pm 0.044$  from A08/A12; after removing the SNe with possible astrometric error, the mean values become  $0.372 \pm 0.047$  and  $0.383 \pm 0.046$ , respectively. Therefore we can conclude that there is no systematic difference between the two studies.

A12 explored some possible biases that might be affecting their sample. First, because of the lower peak luminosity of Type II than Type Ibc SNe, the former may be more difficult to detect in distant galaxies. Additionally, SNe of all types might be more difficult to detect against bright regions (especially the central regions) of host galaxies as the distance increases. The former effect could manifest itself as a decreasing ratio of Type II versus Type Ibc SNe with increasing host galaxy distance and the latter as a decreasing mean NCR value. A12 did detect a trend of decreasing type ratio, but explained this as simply the result of their sample selection effects: their galaxies have been chosen to yield SNe with subtype classifications, which are more unlikely to be determined for distant Type II SNe because of the required systematic photometry. Furthermore, they detected no decrease in mean NCR values with increasing distance for either Type Ibc or Type II, and concluded that there is no selection effect favouring the detection of one over the other against bright regions and that they are thus seeing intrinsic variations in correlation.

Our sample, however, has been chosen based on *galaxy* properties, paying no attention to SN types or subtypes. Therefore it is also worth checking whether we see any trends with increasing distance. The mean NCR values from  $H\alpha$  and  $Ks$ -band images are plotted in Fig. 6 as a function of host galaxy distance. Like A12, we detect no statistically significant decrease in NCR values with distance in either subsample or the full sample in  $H\alpha$  or the  $Ks$  band. The values show some variation, but no obvious trends. Therefore we agree with A12 that there seems to be no selection effect favouring the detection of Type Ibc/IIb SNe over Type II *against bright regions* within our distance limit. In addition, the ratio of Type II SNe versus Ibc/IIb does not significantly drop with increased distance: splitting the sample in half based on distance, we find a ratio of  $1.6 \pm 0.5$  for nearby and  $1.3 \pm 0.4$  for distant galaxies. The Poissonian error bars of the ratios are quite large, and with a sample of this size this result is only tentative.

Furthermore, we have compared the ratio of the main types in our sample to the volumetric SN rates inside a recession velocity limit of  $2000 \text{ km s}^{-1}$  from the Lick Observatory Supernova Search (LOSS) (Smith et al. 2011), and to the relative numbers of SNe within the same limit, discovered between 1998 and 2012.25 and compiled by Eldridge et al. (2013). The ratio of Type II versus Types Ibc/IIb in our sample is  $1.5 \pm 0.3$ , while from the volume-limited LOSS rates we find a ratio of  $1.7 \pm 0.4$  and from Eldridge et al. (2013)  $1.6 \pm 0.3$ . Based on this, we do not seem to have missed a significant number of Type II SNe *compared to Types Ibc/IIb*.

There are significant amounts of dust in the centres of IR-bright galaxies, which can cause up to 80 per cent of SNe to be missed in the nuclear regions of LIRGs (e.g. Mattila et al. 2012; Miluzio et al. 2013). As can be inferred from Fig. 3, the  $Ks$ -band  $Fr$  values show a general central deficit compared to the optical bands. This deficit is dominated by merger and galaxy pair systems, where our sample only includes one SN with  $Fr(Ks) < 0.23$  (19 SNe in total in these galaxies). The indication is that most of the central SNe are missed due to extinction effects for the optical SN searches, but the central  $Ks$ -band light is not due to the reduced extinction in this band. By

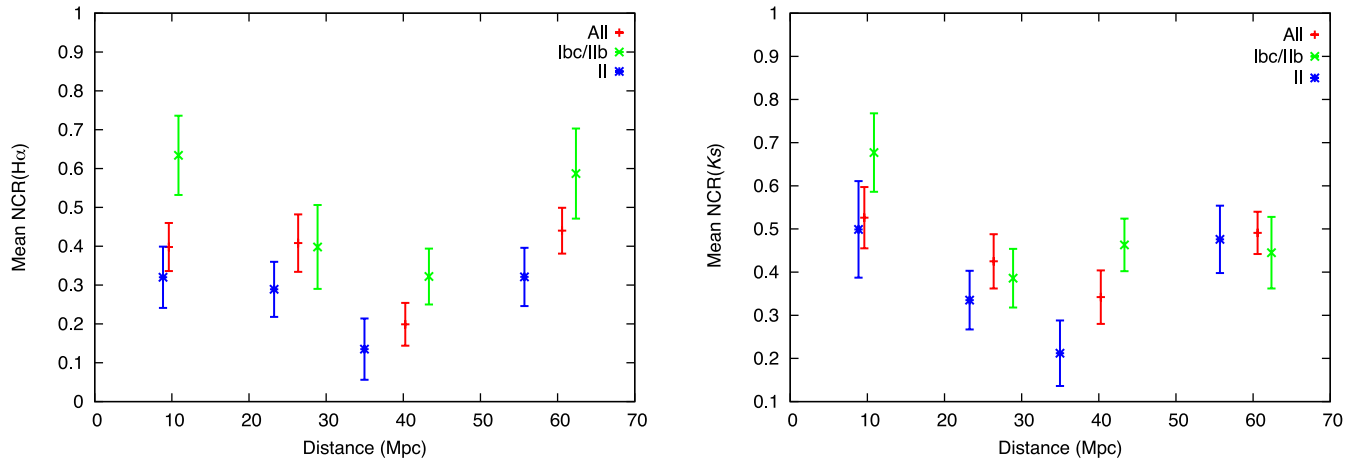


**Figure 6.** The mean NCR values from  $H\alpha$  (left) and  $Ks$ -band (right) images.

eye, the CDF is smoothed out by adding roughly 12 SNe in the  $Fr(Ks)$  range 0–0.25 in the merger sample, resulting in a missed central SN fraction of roughly 90 per cent, which is consistent with the estimates presented by Mattila et al. (2012). In the  $R$  band there is no such deficit, because the central emission suffers from similar extinction as the central SNe. If all the SNe were to be detected, the CDF in  $Ks$  band would resemble the one in  $R$  band, now we see the  $Ks$ -band emission but have not detected the SNe. This effect concerns all types of SNe equally, and thus any bias to our analysis should be insignificant.

## 6.2 Differences between the SN types

Type Ibc/Iib SNe occur significantly closer to regions of recent star formation than Type II SNe. The average  $NCR(H\alpha)$  value for Ibc/Iib is  $0.475 \pm 0.052$ , which indicates they closely follow the distribution of  $H\alpha$  light. Comparing the distribution of Type Ibc/Iib SNe and a flat distribution of NCR values with the KS test confirms this association. Type II SNe, on the other hand, do not follow the star-forming regions. A KS test between the two main types indicates that they arise from different stellar populations. Earlier studies (e.g. A08, A12) explain this with Type Ibc SNe having more massive progenitors which thus have shorter lifetimes and therefore have less time to drift away from their birthplaces, or the  $H II$  region has less time to dissipate, leading to a closer association with star-forming regions. In addition, as more SNe occur in an  $H II$  region, it will gradually cease to exist due to loss of stars emitting ionizing radiation and strong stellar winds and the SN explosions blowing away the gas. Therefore the first SNe would show a stronger association with the region (as discussed by A12).

When we examine the subtypes Ib and Ic separately, we find that the  $NCR(H\alpha)$  values of our Type Ib SNe are consistent with those of Type II, while those of Type Ic are confirmed to be significantly higher – too high, in fact, to be randomly drawn from the  $H\alpha$  emission; they are strongly correlated with the  $H II$  regions. The difference between Types Ib and II is rather small in A12 as well – in fact, the error limits of their mean NCRs overlap slightly. This indicates an overlapping mass range for the progenitors of Types Ib and II, or at least that they both are outside the lifetime range traced by  $H\alpha$  emission.

A caveat was recently discussed by Crowther (2013). He argued that since individual small  $H II$  regions would dissipate in a time-

scale shorter than the ages of the progenitors of Type Ibc/Iib or II SNe, no meaningful constraints could be obtained for stars less massive than 50–100  $M_{\odot}$ ; in addition, small  $H II$  regions would not be detected in the ground-based images used for this study. On the other hand, giant  $H II$  regions would last on the order of 20 Myr, meaning that one can only make weak constraints based on association with  $H\alpha$  emission, namely, limits of  $\geq 12 M_{\odot}$  for SE-SN progenitors and  $\geq 8 M_{\odot}$  for Type II, based on what is considered the smallest possible mass for a SN progenitor. The differences in correlation with  $H\alpha$  light that are seen in both our study and those in James & Anderson (2006) and later papers do indicate that Type Ic progenitors are more massive than the 12  $M_{\odot}$  limit while some Ib and II progenitors could be less massive.

One way to address this problem is to also use UV light as an indicator of *recent*, on time-scales of 16 to 100 Myr (Gogarten et al. 2009), as opposed to *on-going*, star formation. This was done for Type II-P and II-n SNe and ‘impostors’ in A12. Based on our results, we find that Type II SNe accurately trace the galaxy NUV light with a mean  $NCR(NUV)$  close to 0.5. We obtained a mean  $NCR(NUV)$  close to 0.5 (consistent with Type II) for Type Ib and a significantly higher one (confirmed by the KS test against a flat distribution) for Ic. Thus, Type Ic SNe preferably occur in regions with high NUV intensity. This lends additional support to Type Ic progenitors being of higher mass than those of Types Ib and II. Since the difference between Types Ib and II in both  $H\alpha$  and NUV is insignificant and they both are consistent with being randomly drawn from the NUV light distribution, this indicates that their progenitor lifetimes are  $> 16$  Myr as traced by the NUV (Gogarten et al. 2009). Lower-mass interacting binaries, instead of massive Wolf–Rayet stars, have been proposed to be the progenitors of a significant fraction of Type Ibc SNe (e.g. Podsiadlowski, Joss & Hsu 1992; Smartt 2009) and of Type Iib SNe (Maund et al. 2004), which is also supported by a lack of direct detections of their progenitors (Eldridge et al. 2013). Smith et al. (2011) and Dessart et al. (2012) suggested that Type Ib and Iib SNe arise mostly from interacting binaries and Type Ic SNe at least partly from more massive single WR stars. This could explain our results.

Our  $R$ -band results are very similar to NUV. The KS test shows a significant difference between the SNe of Types Ibc/Iib – and specifically Ic – and a flat distribution of  $NCR(R)$  values. The calculated mean values for Types II and Ib are close to 0.5, while Ic SNe are concentrated into the bright areas. It is likely, however,

that  $R$ -band light does not provide a useful indicator on SN environments, since it includes both the  $H\alpha$  line emission and a stellar continuum from different sources.

$Ks$ -band light is thought to be a good tracer of stellar mass i.e. old stars (Mannucci et al. 2005) since, in normal galaxies, most of the mass is in older stars. However, the contribution of red supergiants to the  $Ks$ -band light, which also exists in normal spiral galaxies (Kotilainen et al. 2012), dominates this band in starburst galaxies (Engelbracht et al. 1998), which would make  $Ks$ -band light a useful indicator of recent star formation similar to  $H\alpha$ . In the  $Ks$  band our results are indeed similar to those in  $H\alpha$ : the mean NCR for Type Ic is significantly larger than for Type II, while Types Ib and II are consistent with each other. The KS test confirms this. Additionally there is a significant difference from a flat distribution for Type II, but not for other types. Furthermore,  $Ks$ -band emission is much less affected by extinction than  $H\alpha$ , which we can see in the difference between  $Fr$  values; smaller  $Fr$  values could be expected in  $H\alpha$  than in  $Ks$ -band because of the central  $H\alpha$  flux being strongly absorbed by the dust. Extinction could have an effect on NCR values as well. However, this similarity in NCR values suggests that the lack of extinction correction makes no great difference here, assuming that  $Ks$ -band light does trace the birthplaces of massive stars in actively star-forming galaxies.

As for the radial ( $Fr$ ) distributions of the CCSNe, the KS test finds no statistically significant excess of Type Ibc/IIb SNe in the inner regions of galaxies compared to the host galaxy emission in the optical bands, which can also be seen in Fig. 3. Our mean  $Fr(H\alpha)$  values are consistent with those of the SNe in Habergham et al. (2012) within the errors for all types, however. In the  $Ks$  band we see a difference between Type II and a flat distribution, but no difference between Types Ibc/IIb and a flat distribution. However, the radial distribution of optically detected SNe is not ‘supposed’ to be flat in this band (see Section 6.1), and thus the difference between Type II SNe and a flat distribution does not necessarily indicate an outer excess of Type II SNe.

However, the mean normalized radial distances and the scale length of the SN surface density are significantly shorter for Types Ibc/IIb than for Type II. These results indicate that SNe of Type Ibc/IIb are indeed more concentrated to the central regions of galaxies than those of Type II, which is in agreement with previous results by e.g. Hakobyan et al. (2009) and Habergham et al. (2012). Furthermore, the radial distances for Types Ib and Ic are equal within the errors, meaning that here we do see a difference between Types Ib and II. The different results from these two tests may be explained by the fact that they measure different things. The normalized radial distances are not affected by the properties of the central regions, while  $Fr$  values are.

### 6.3 Differences between normal spirals and IR-bright galaxies

The clearest difference we see in the distributions of CCSNe in normal versus IR-bright galaxies is in the scale length of their surface density. Based on a MC analysis, we find a normalized scale length of  $\tilde{h}_{\text{SN}} = 0.23^{+0.03}_{-0.02}$ , which is statistically significantly smaller than that derived by Hakobyan et al. (2009) for a sample of CCSNe in spiral galaxies ( $0.29 \pm 0.01$ ). However, there are roughly five ‘extra’ Ibc SNe in the central regions compared to what one would expect from an exponential surface density profile derived by ignoring the innermost radial distance bin. Since by ignoring the central bin we obtained a similar scale length ( $0.24^{+0.05}_{-0.04}$ ) for Types Ibc/IIb as Hakobyan et al. (2009) did for their Type Ibc sample ( $0.24 \pm 0.02$ ), and since the Type II scale lengths match within the

errors [we get  $\tilde{h}_{\text{SN}} = 0.29^{+0.06}_{-0.04}$  and Hakobyan et al. (2009) report  $0.31 \pm 0.02$ ], the indication is that our shorter overall scale length is mainly due to an excess of Types Ibc/IIb in the central regions, with respect not only to Type II but also to Types Ibc/IIb in normal galaxies.

Prior radial analysis papers, and our corresponding results, indicate more central positions for SNe of Type Ibc/IIb than for other Type II. A metallicity gradient is often brought up as an explanation (e.g. Anderson & James 2009; Hakobyan et al. 2009), since metallicity is known to be a major factor in the mass-loss rates of the progenitor stars (e.g. Crowther et al. 2002).

‘Disturbed’ galaxies, especially merger systems, have a less pronounced metallicity gradient than normal isolated galaxies (e.g. Rich et al. 2012). Dividing the galaxy sample into isolated, disturbed and merging/closely paired systems (see Section 2), we see that Type Ibc SNe are more centrally located in ‘disturbed’ galaxies. The mean  $R_{\text{SN}}/R_{25}$  for Types Ibc/IIb is  $0.588 \pm 0.138$  in isolated galaxies,  $0.315 \pm 0.085$  in ‘disturbed’ ones and  $0.227 \pm 0.050$  in merging/close-pair systems. Thus Type Ibc/IIb SNe in mergers and ‘disturbed’ galaxies are significantly more centralized. This is consistent with what is seen by Habergham et al. (2012), but it is the opposite of what one would expect if metallicity was the deciding factor, since the central metallicity in ‘disturbed’ galaxies is expected to be *lower* than in isolated galaxies. Rich et al. (2012) also show that the metallicity gradient gets less pronounced with increased IR luminosity. However, we divided our sample into (relatively) IR-luminous and IR-faint galaxies, the threshold being the median  $\log L_{\text{FIR}}$  of our sample (10.57) with 44 SNe in the brighter half and 42 in the fainter half. We find that the radial distances for Type Ibc/IIb SNe are the same, within the errors, regardless of which subsample the host galaxy belongs to (mean  $R_{\text{SN}}/R_{25} = 0.359 \pm 0.089$  in the fainter galaxies and  $0.344 \pm 0.072$  in the brighter ones). Thus we see no evidence of a metallicity effect driving the relative centralization of Type Ibc/IIb SNe.

In the study of Habergham et al. (2012) the centralization is taken to indicate that in the central regions of ‘disturbed’ galaxies, the IMF is top-heavy. Klessen, Spaans & Jappsen (2007) presented a model, based on numerical simulations, where the increased temperature in intensely star-forming regions causes the local Jeans mass to increase, which would in turn result in a top-heavy IMF with a peak around  $15 M_{\odot}$ . Obviously this would affect strongly star-forming galaxies more than normal spirals. However, we are seeing both Ib and Ic SNe in the central regions (four of Type Ib and five of Type Ic inside  $0.2R_{25}$ ; see also Table 7). According to our NCR results, the mass ranges of the progenitors of Type II and Ib SNe seem to overlap strongly. Thus, while the enhanced fraction of Type Ic SNe can be explained by a modified IMF in the central regions, that of Type Ib SNe seemingly cannot. Thus our results suggest that while the top-heavy IMF may play a role, it is not the only factor behind the enhanced SE fraction in the central regions.

Since we see no evidence of a metallicity dependence in the centralization, and since relatively low-mass binaries probably form a significant fraction of Type Ib(c) progenitors (see Section 6.2), we suggest that an enhanced close binary fraction in areas of high star formation density could be a significant factor, perhaps along with the top-heavy IMF to account for the prevalence of both Ib and Ic SNe. King et al. (2012) showed that in young star-forming regions in the Milky Way, the fraction of binary systems as a whole is either very weakly decreased or not at all compared to the field, while the fraction of *close* binaries is significantly enhanced. Furthermore, a large fraction of star formation happens in young massive star clusters (Portegies Zwart, McMillan & Gieles 2010), which have

been shown by Rangelov et al. (2012) to correlate with X-ray binaries. Our sample galaxies tend to have strong central star formation, meaning that this would also apply to the central regions. In such dense regions found inside clusters, primordial hard binaries (those with high binding energy) tend to harden and soft ones tend to soften according to Heggie's law (Heggie 1975). While some of these binaries do get disrupted, this probably will not happen until many of them have exploded as SNe.

The relative numbers of SNe of different types might also offer an indicator of differences between IR-bright and normal galaxies. As already stated in Section 6.1, the ratio of the numbers in our main subsamples (II versus Ibc/Iib) should be  $1.6 \pm 0.3$  (or  $1.7 \pm 0.4$ ), based on the volume-limited numbers of different types of SNe inside the recession velocity limit of  $2000 \text{ km s}^{-1}$ , according to Eldridge et al. (2013) (or Smith et al. 2011). In our sample, the observed ratio is  $1.5 \pm 0.3$ , and thus in agreement with the volume-limited samples. If the central 'extra SNe' mentioned above are excluded, our type ratio would be  $1.6 \pm 0.4$ . This indicates the rate of Type Ibc/Iib SNe compared to Type II in IR-bright galaxies is not significantly different than in normal galaxies. The suggested excess of Type Ibc/Iib SNe in the central regions *compared to normal galaxies* is thus not strong enough to affect the relative rates significantly.

## 7 CONCLUSIONS

We have presented results for correlations between CCSNe of different types and light in the  $H\alpha$ ,  $R$  band,  $Ks$  band and NUV in IR-bright galaxies. We have also presented an analysis of radial positions of these SNe in relation to the host galaxy light, and fitted functions to describe the SN surface densities. We have, when possible, compared these results with earlier studies, with samples dominated by normal spiral galaxies.

Our results confirm that Type Ic SNe show a higher correlation with  $H\alpha$  light (and thus on-going star formation) than Types II or Ib. In the NUV (recent star formation) Types II and Ib accurately trace the host galaxy light, while Ic SNe are concentrated in the bright regions. Assuming that a higher correlation with  $H\alpha$  light is because of a shorter lifetime of the progenitor star and thus a higher mass, the average masses of Type Ic progenitors are indicated to be higher than those of Types Ib and II, as asserted previously by e.g. A08 and A12. However, both Type Ib and II are consistent with being randomly drawn from the NUV light distribution but not from the  $H\alpha$  distribution; thus the mass difference between these progenitors may not be significant, and instead binarity may play a larger role.

In the  $Ks$  band, the pixel statistics results are quite similar; Type Ibc/Iib SNe are more strongly correlated with the underlying galaxy light. Since the  $Ks$ -band light of actively star-forming galaxies is dominated by red supergiants, it is also a tracer of recent star formation in these galaxies. Therefore we can infer the same results as from the  $H\alpha$  and NUV data, further supported by the weaker extinction in the IR.

Type Ibc/Iib SNe are preferentially more centrally located in their host galaxies than Type II in our sample, which is consistent with previous results by Habergham et al. (2012). This is probably due to the effect of an enhanced close binary fraction and/or a top-heavy IMF in the central regions compared to the outer regions (however, the IMF *alone* seems inadequate to explain our results). We see no evidence of metallicity playing a major role here. A significant fraction of SNe may be missed in the centres of IR-bright galaxies due to high line-of-sight extinctions and contrast effects, which we see clearly when comparing the CCSN distribution with that of host

galaxy  $Ks$ -band light, but we do not find any evidence that Type II SNe would be more strongly affected by this than Type Ibc/Iib in our sample.

The scale length of the CCSN surface density is significantly smaller in IR-bright galaxies than in samples dominated by normal spiral galaxies. Furthermore, this seems to be caused mainly by an excess of Type Ibc/Iib SNe in the central regions, compared not only to Type II but also to normal spiral galaxies as well: by ignoring the central SNe the scale lengths for both main types (Ibc/Iib and II) match those derived by Hakobyan et al. (2009). The top-heavy IMF and/or enhanced close binary fraction thus especially apply to IR-bright galaxies, many of which are 'disturbed'. If dust extinction in these galaxies is greater than normal and more (central) SNe are missed, this effect is even stronger than what is seen here.

## ACKNOWLEDGEMENTS

We thank the anonymous referee for his or her very useful comments. We also thank Phil James and Joe Anderson for their comments and constructive discussion, Stacey Habergham for sharing the  $F_r$  values from her paper, Rubina Kotak and Justyn Maund for discussion on biases, Andrew Thompson for providing a copy of his MSc thesis for that discussion, and José Ramon Sánchez-Gallego and Johan Knapen for sharing their optical images of four galaxies. EK acknowledges financial support from the Jenny and Antti Wihuri Foundation. PV acknowledges support from the National Research Foundation.

Based on observations made with the NOT, operated on the island of La Palma jointly by Denmark, Finland, Iceland, Norway and Sweden, in the Spanish Observatorio del Roque de los Muchachos of the Instituto de Astrofísica de Canarias. The data presented here were obtained in part with ALFOSC, which is provided by the Instituto de Astrofísica de Andalucía (IAA) under a joint agreement with the University of Copenhagen and NOTSA. The *WHT* is operated on the island of La Palma by the ING in the Spanish Observatorio del Roque de los Muchachos of the Instituto de Astrofísica de Canarias.

This research has made use of the NASA/IPAC Extragalactic Database (NED) which is operated by the Jet Propulsion Laboratory, California Institute of Technology, under contract with the National Aeronautics and Space Administration. We acknowledge the usage of the HyperLeda data base (<http://leda.univ-lyon1.fr>).

## REFERENCES

- Alard C., 2000, *A&AS*, 144, 363
- Alard C., Lupton R. H., 1998, *ApJ*, 503, 325
- Anderson J. P., James P. A., 2008, *MNRAS*, 390, 1527 (A08)
- Anderson J. P., James P. A., 2009, *MNRAS*, 399, 559
- Anderson J. P., Habergham S. M., James P. A., 2011, *MNRAS*, 416, 567
- Anderson J. P., Habergham S. M., James P. A., Hamuy M., 2012, *MNRAS*, 424, 1372 (A12)
- Barbon R., Cappellaro E., Turatto M., 1989, *A&AS*, 81, 421
- Crowther P. A., 2013, *MNRAS*, 428, 1927
- Crowther P. A., Dessart L., Hillier D. J., Abbott J. B., Fullerton A. W., 2002, *A&A*, 392, 653
- Dessart L., Hillier D. J., Gezari S., Basa S., Matheson T., 2009, *MNRAS*, 394, 21
- Dessart L., Hillier D. J., Li C., Woosley S., 2012, *MNRAS*, 424, 2139
- Drapar P. W., Berry D. S., Jenness T., Economou F., 2009, *ASP Conf. Ser.* Vol. 411. *Astronomical Data Analysis Software and systems XVIII*. Astron. Soc. Pac., San Francisco, p. 575

- Eldridge J. J., Fraser M., Smartt S. J., Maund J. R., Crockett R. M., 2013, *MNRAS*, 436, 774
- Engelbracht C. W., Rieke M. J., Rieke G. H., Kelly D. M., Achtermann J. M., 1998, *ApJ*, 505, 639
- Filippenko A. V., 1997, *ARA&A*, 35, 309
- Freeman K. C., 1970, *ApJ*, 160, 811
- Gogarten S. M. et al., 2009, *ApJ*, 691, 115
- Habergham S. M., Anderson J. P., James P. A., 2010, *ApJ*, 717, 342
- Habergham S. M., James P. A., Anderson J. P., 2012, *MNRAS*, 424, 2841
- Hakobyan A. A., Mamon A., Petrosian A. R., Kunth D., Turatto M., 2009, *A&A*, 508, 1259
- Heggie D. C., 1975, *MNRAS*, 173, 729
- Herrero-Illana R., Pérez-Torres M. Á., Alberdi A., 2012, *A&A*, 540, L5
- James P. A., Anderson J. P., 2006, *A&A*, 453, 57
- Kankare E. et al., 2012, *MNRAS*, 424, 855
- Kelly P. L., Kirshner R. P., 2012, *ApJ*, 759, 2012
- Kennicutt R. C., 1998, *ARA&A*, 36, 189
- King R. R., Goodwin S. P., Parker R. J., Patience J., 2012, *MNRAS*, 427, 2636
- Klessen R. S., Spaans M., Jappsen A.-K., 2007, *MNRAS*, 374, L29
- Kotilainen J. K., Hyvönen T., Reunanen J., Ivanov V. D., 2012, *MNRAS*, 425, 1057
- Li W., Filippenko A. V., Van Dyk S. D., Hu J., Qiu Y., Modjaz M., Leonard D. C., 2002, *PASP*, 114, 403
- Li W., Van Dyk S. D., Filippenko A. V., Cuillandre J.-C., Jha S., Bloom J. S., Riess A. G., Livio M., 2006, *ApJ*, 641, 1060
- Manchado A. et al., 2004, in Moorwood A. F. M., Masanori I., eds, *Proc. SPIE Vol. 5492, Ground-based Instrumentation for Astronomy*. SPIE, Bellingham, p. 1094
- Mannucci F., Della Valle M., Panagia N., Cappellaro E., Cresci G., Maiolino R., Petrosian A., Turatto M., 2005, *A&A*, 433, 807
- Mattila S., Meikle W. P. S., 2001, *MNRAS*, 324, 325
- Mattila S., Meikle W. P. S., Greimel R., 2004, *New Astron. Rev.*, 48, 595
- Mattila S., Smartt S. J., Eldridge J. J., Maund J. R., Crockett R. M., Danziger I. J., 2008, *ApJ*, 688, L91
- Mattila S. et al., 2012, *ApJ*, 756, 2012
- Maund J. R., Smartt S. J., Kudritzki R. P., Podsiadlowski Ph., Gilmore G. F., 2004, *Nat*, 427, 129
- Maund J. R. et al., 2011, *ApJ*, 739, L37
- Miluzio M. et al., 2013, *A&A*, 554, A127
- Packham C. et al., 2003, *MNRAS*, 345, 395
- Paturel G., Petit C., Prugniel Ph., Theureau G., Rousseau J., Brouty M., Dubois P., Cambrésy L., 2003, *A&A*, 412, 45
- Petrosian A. et al., 2005, *AJ*, 129, 1369
- Podsiadlowski Ph., Joss P. C., Hsu J. J. L., 1992, *ApJ*, 391, 246
- Portegies Zwart S. F., McMillan S. L. W., Gieles M., 2010, *ARA&A*, 48, 431
- Prieto J. L., Stanek K. Z., Beacom J. F., 2008, *ApJ*, 673, 999
- Rangelov B., Chandar R., Prestwich A., Whitmore B. C., 2012, *ApJ*, 758, 99
- Rich J. A., Torrey P., Kewley L. J., Dopita M. A., Rupke D. S. N., 2012, *ApJ*, 753, 5
- Sánchez-Gallego J. R., Knapen J. H., Wilson C. D., Barmby P., Azimlu M., Courteau S., 2012, *MNRAS*, 422, 3208
- Sanders D. B., Mazzarella J. M., Kim D.-C., Surace J. A., Soifer B. T., 2003, *AJ*, 126, 1607
- Smartt S. J., 2009, *ARA&A*, 47, 63
- Smartt S. J., Maund J. R., Hendry M. A., Tout C. A., Gilmore G. F., Mattila S., Benn C. R., 2004, *Sci*, 303, 499
- Smith N., Li W., Filippenko A. V., Chornock R., 2011, *MNRAS*, 412, 1522
- Van Dyk S. D., Peng C. Y., King J. Y., Filippenko A. V., Treffers R. R., Li W., Richmond M. W., 2000, *PASP*, 112, 1532
- Van Dyk S. D. et al., 2011, *ApJ*, 741, L28
- Véron-Cetty M.-P., Véron P., 1998, *ESO Scientific Report Series No. 18, A Catalogue of Quasars and Active Nuclei*, 8th edn. European Southern Observatory. Garching
- Wada K., Norman C. A., 2002, *ApJ*, 566, L21

This paper has been typeset from a  $\text{\TeX}/\text{\LaTeX}$  file prepared by the author.